# NUMERICAL ANALYSIS OF FREEZING BEHAVIOR OF SATURATED CEMENTITIOUS MATERIALS WITH DIFFERENT AMOUNTS OF CHLORIDE

# NUMERISCHE ANALYSE DES FROSTVERHALTENS GESÄTTIGTER ZEMENTGEBUNDENER MATERIALIEN MIT UNTERSCHIEDLICHEN CHLORIDANTEILEN

Sekandar Zadran, Joško Ožbolt, Serena Gambarelli

*Materials Testing Institute (MPA), University of Stuttgart, Otto-Graf-Institute*

## ABSTRACT

The freezing behavior of cement paste saturated with different chloride concentrations is investigated numerically with a coupled 3D hygro-thermo-mechanical FE analysis. The mathematical formulation of the freezing processes in the context of poromechanics takes into account the water (hydraulic) and ice pore pressure as well as the distribution of heat (temperature) and strains. These quantities are calculated numerically based on three coupled differential equations, namely the static equilibrium equation and the equations for the transport of water and heat. The coupling between the mechanical (loading) and the non-mechanical processes (freezing) is performed using a staggered solution scheme. The proposed numerical approach is first validated using numerical and experimental studies from the literature dealing with two different cement pastes saturated with different amounts of chloride. The validated model is then used to investigate the effects of liquid water permeability, total porosity, and pore size distribution on the freezing behavior of hardened cement paste. The results show that liquid water permeability has a strong effect on the pore pressure and deformation of the hardened cement paste. It is also shown that by decreasing the total porosity, the material becomes denser and contracts more as the temperature decreases, leading to a decrease in freezing strain.

# ZUSAMMENFASSUNG

Das Frostverhalten von Zementstein, der mit unterschiedlichen Chloridkonzentrationen gesättigt ist, wird numerisch mit einer gekoppelten 3D hygro-thermo-mechanischen FE-Analyse untersucht. Die mathematische Formulierung der Frostprozesse im Rahmen der Poromechanik berücksichtigt den Wasser- (hydraulischen) und Eis-Porendruck sowie die Verteilung von Wärme (Temperatur) und Dehnungen. Diese Parameter sind numerisch auf der Basis von drei gekoppelten Differentialgleichungen berechnet, nämlich der statischen Gleichgewichtsgleichung und den Gleichungen für den Transport von Wasser und Wärme. Die Kopplung zwischen den mechanischen (Belastung) und den nicht-mechanischen (Frost) Prozessen erfolgt über ein versetztes Lösungsschema. Der vorgeschlagene numerische Ansatz wird zunächst anhand numerischer und experimenteller Studien aus der Literatur validiert. Sie befassen sich mit zwei verschiedenen Zementsteinen, die mit unterschiedlichen Mengen an Chlorid gesättigt sind. Das validierte Modell wird dann verwendet, um die Auswirkungen der Wasserdurchlässigkeit, der Porosität und der Porengrößenverteilung auf das Frostverhalten von Zementstein zu untersuchen. Die Ergebnisse zeigen, dass die Wasserdurchlässigkeit einen starken Einfluss auf den Porendruck und die Deformation des Zementsteins hat.

Es wird auch gezeigt, dass durch eine Verringerung der Gesamtporosität das Material dichter wird und sich bei sinkender Temperatur mehr zusammenzieht, was zu einer Reduzierung der Frostdehnungen führt.


# 1. INTRODUCTION

Frost damage is one of the most important factors affecting the durability of cementitious materials in regions with cold climates. Over the years, many theories have been proposed to explain this complex phenomenon [1]. According to Powers, the increase in hydraulic pressure due to the increase in the volume of water during the transformation to ice leads to internal stresses in the pores, which cause the damage of cementitious materials [2]. During frost action, after the conversion of water to ice, there is a 9 % increase in volume with subsequent water expulsion from the freezing pores to the unfrozen pores. However, Scherer [3] emphasized that the crystallization pressure of the ice and not the hydraulic pressure should be the predominant source of stresses during freezing.

Damage due to frost action can be categorized as internal cracking and surface scaling [4]. Internal cracking leads to lower material modulus of elasticity, drop in tensile strength and increase in porosity and permeability [5]. Internal damage affects the concrete mass and is characterized by significant microcracking of the cement paste and weakening of bond between the solid matrix and particles. Under freeze-thaw cycles, calcium-silicate-hydrate (C-S-H) remains stable, however, the portlandite (Ca(OH)2) and sulfoaluminates are partly dissolved and recrystallized in the air voids of the cement paste as fibrous secondary hydrates after repeated freeze-thaw cycles [6]. Surface scaling, which is most commonly associated with the presence of solutes, results in material surface loss at a solute concentration of roughly 3 % [7].

The freezing behavior of cement-based materials under fully saturated condition has been experimentally investigated by a number of researchers. Zeng et al. [8] analysed both numerically and experimentally the behavior of two cement pastes saturated with different amount of chloride concentrations. Based on their experimental results, the ice saturation degree is influenced by both porosity and pore connectivity. The freezing strains during the first cooling phase obtained from the numerical simulations of the poroelastic model show a good agreement with the measured strains. To experimentally investigate the freeze-thaw induced damage and changes in the pore structure of cement mortar, a recent study was carried out by Wang et al. [9] using low-field NMR. Additionally, in order to establish the connection between freeze-thaw damage and pore structure degradation, the complete deterioration of mortar specimens was also observed. Zhang et al. [10] performed experimental study on the mechanical properties and pore structure degradation of concrete under freeze-thaw cycles with two different water to cement ratios, 0.45 and 0.55. Each freeze-thaw cycle lasted 3-4 h with a maximum number of 200 cycles.

Several models have been developed over the years to predict the thermo-mechanical behavior of porous building materials such as cement paste subjected to frost action. Powers introduced the famous hydraulic pressure and osmotic pressure theories, which constructed the basic theory of frost damage [11, 12]. A mathematical model based on the pore size distribution and desorption and absorption isotherms for concrete below and above 0°C was established by Bažant et al. [13]. On the basis of poromechanics and local thermodynamic equilibrium conditions between various phases, Zuber et al. [14, 15] presented a numerical model that

can be implemented into a finite element (FE) code to predict the behavior of completely saturated cement-based materials subjected to freezing temperatures. The FE model proposed by Zuber et al. was used in [15] to predict the volume instability of hydrated cement systems upon freezing. Yang et al. [16] proposed a micromechanical model to simulate the expansion of cement paste, which takes into account the thermal dilation of the matrix and pressure in the pore space.

Based on the HYMOSTRUC3D hydration model, Liu et al. [17] generated virtual cement pastes with integrated crystallization pressure due to ice formation. This method enables the visualization of cracks and ice in the cement paste. To quantitatively investigate the mechanism of chloride diffusion under FTCs, a 2D 3-phases mesoscopic numerical model on chloride diffusion in concrete subjected to freeze-thaw attack was proposed by Jiang et al. [18]. By using a time-dependent variable called porosity, which reflects how freeze-thaw action affects the concrete pore structure and couples the freeze-thaw process with the chloride diffusion process at a temporal scale, this model takes into account the FTCs-induced damage affected by chloride diffusion. Rhardane et al. [19] introduced a thermo-mechanical model based on thermodynamic considerations and physical processes at the microscale to provide a quantitative assessment of the mechanisms caused by the freeze–thaw action in relation to the internal damage of cementitious materials.

Despite proposed models by several researchers, freezing process in porous media, such as concrete, still remains a very complex topic. The process involves interaction between heat transfer and moisture, phase change and deformation. Heat-moisture migration was studied by Olsen [20], whereas hygro-mechanical coupling has been studied by Zuber and Marchand [14]. However, only few studies are available in the literature on the coupled thermo-hygro-mechanical behavior of concrete under freezing.

The main objective of the present study is to numerically investigate the freezing behavior of two different cement pastes saturated with different chloride concentrations. The mathematical formulation of the model is based on the theory available in the literature [14]. The 3D coupled hygro-thermo-mechanical (HTM) model [21] implemented in the in-house FE code MASA [22] is used as a framework for the calculations. The mechanical part of the model is based on the microplane theory [23], suitable for the non-linear analysis of different materials, i.e. cement paste. However, in the present study, the material is considered as linear

elastic. The coupling between the mechanical (loading) and non-mechanical processes (freezing), is ensured by using the staggered solution procedure. The model is first validated against a numerical and experimental study available in the literature [8]. The validated model is then used in the parametric study to investigate the effect of liquid water permeability, total porosity and pore size distribution on the freezing behavior of the material.

## 2. MATHEMATICAL FORMULATION OF THE MODEL

When a porous material is subjected to freezing, cryo-deformation occurs as a result of several combined effects: (i) the difference in density between the liquid water and the ice crystal; this difference in density causes the expansion of the solid matrix surrounding the forming crystal and the displacement of some of the liquid water from the freezing sites toward the pores still filled with liquid water; (ii) the surface tension created between the various constituents, which ultimately determines the crystallization process in conjunction with the pore radius distribution; (iii) the drainage of liquid water displaced from the freezing sites toward the air pores; (iv) the cryo-suction process that drives liquid water toward the already frozen sites as the temperature continues to drop; (v) the thermomechanical coupling between the pressurized pore space and the surrounding solid matrix that determines the overall cryo-deformation [24].

The freezing behavior of cementitious materials is studied by a poromechanical approach. The material is considered as a porous medium saturated with water and subjected to freezing. The thermodynamic laws involved are used to establish the constitutive equations for phase change, mass transfer and heat transfer. As a result, the pore pressure generated by freezing is converted into a macroscopic effective stress by a homogenization scheme. In the proposed model, the material is assumed to be fully saturated and linearly elastic. The governing variables are the pressure in the water fluid (pw), the temperature (T), and the strains (ε). The mathematical formulation of the freezing of a porous continuum is in principle the same as that presented by Zuber and Marchand [14]. The model is extended here with respect to the influence of chloride content on the freezing mechanism of porous materials.

## 2.1 Continuity Equation

Based on Darcy's constitutive law and the mass balance of the porous media with accounting for the influence of the coupling between deformation, ice formation, and heat and water migration, the constitutive equation for the pressure in the liquid water was formulated by Zuber and Marchand [14]:

$$\beta \dot{p}_w = \nabla \cdot \left( \frac{D}{\eta} \nabla p_w \right) + S - b\dot{\varepsilon}_v \tag{1}$$

where $p_w$ = pressure in the liquid water; $D$ = permeability (m$^2$) of the porous media; $\eta$ = fluid viscosity (Pa sec); $\varepsilon_v$ = volumetric strain of the medium; $b$ = Biot's coefficient (dimensionless) and:

$$\beta = \left( \frac{nS_w}{K_w} + \frac{nS_i}{K_i} + \frac{b-n}{K_m} \right), = \left( \frac{1}{\rho_i} - \frac{1}{\rho_w} \right) \dot{w}_i + \overline{\alpha}\dot{T} - \frac{b-n}{K_m}\dot{X} - \frac{nS_i}{K_i}\gamma\dot{\kappa} \tag{2a}$$

$$\overline{\alpha} = nS_w\,\alpha_w + nS_i\ \ \alpha_i + (b-n)\alpha_0 \tag{2b}$$

$$R_{peq} = R_{eq} + \delta, R_{eq} = \frac{2\tau\, cos\Theta}{\rho_i\, S_f |\theta|}, \delta = 1.97|\theta|^{-\frac{1}{3}}, \theta = T_f - T_0 \tag{2c}$$

$$\kappa = \frac{2}{R_{eq}}, X = \frac{\tau}{n} \int_{\infty}^{R_{peq}} \left( \kappa - \frac{1}{r-\delta} \right) \frac{d\varphi}{dr} dr, \varphi(r) = \int_{r}^{\infty} \frac{d\varphi}{dr} dr \tag{2d}$$

in which $n$ = total porosity of a given mixture (m$^3$/m$^3$); $r$ = effective pore radius (m); $\varphi(r)$ = cumulative volume of pores with radius greater than $r$ (m$^3$/m$^3$); $T_f$ = freezing temperature of pore water (K); $T_0$ = normal freezing temperature of bulk water (273.15 K); $S_i$ and $S_w$ = proportions of the porosity filled with ice and liquid water, respectively ($S_i$+$S_w$ = 1); $K_w$ and $K_i$ = compressibility modulus of water and ice (Pa), respectively; $K_m$ = compressibility modulus of the solid matrix (Pa); $\rho_i$ = mass density of ice (kg/m$^3$); $\rho_w$ = mass density of water (kg/m$^3$); $w_i$ = mass of frozen water (kg/m$^3$); $X$ = pressure which is related to the presence of ice in the frozen pores (Pa); $\kappa$ (curvature) accounts for the effects of the spherical interface between liquid water and ice (m$^{-1}$) (note that 2 stays for cylindrical pores); $\alpha_w$ and $\alpha_i$ = volumetric thermal dilatation of water; and ice (K-1), respectively; $\alpha_0$ and $\overline{\alpha}$ = volumetric thermal dilatation of bulk skeleton and of the system (K$^{-1}$), respectively; $R_{peq}$ = equilibrium (critical) pore radius (nm); $R_{eq}$ = radius of curvature of the liquid/ice interface (nm); $\delta$ = thickness of the liquid-like layer between the pore ice surface and matrix that remains unfrozen (nm); $\tau$ = surface tension of ice/water interface (N/m): $\Theta$ = contact angle between the crystal

and pore wall calculated from Fig. 1a (degree); $S_f$ = Fusion entropy density of ice (J/(K kg)).

### 2.1.1 Equilibrium pore radius

The pore structure of a porous medium (cement paste) has a great influence on the frost resistance of the material [8]. During the cooling process, the water trapped in the pores can freeze at different temperatures depending on the pore size. The smaller the pore radius, the lower the temperature at which the ice forms. When the temperature drops below the freezing point of water ($T_0$), ice crystals initially form in the larger pores. With further decrease of temperature, the ice crystals also begin to form in the small pores. An important aspect is the surface interaction between the matrix and the pore water or pore ice, as it causes freezing depression.

Due to the surface contributions to the free energy, the freezing point decreases with decreasing pore size. The equilibrium (critical) pore radius ($R_{peq}$) at which water in the pores starts freezing when the temperature $\theta$ (in degrees Celsius) is reached is calculated based on the well-known Gibbs-Thomson equation for pure water (Eq. (2c)). It represents the relationship between the equilibrium pore radius at a given temperature $T$ below which ice cannot be formed [25]. The existence of the water layer ($\delta$) between the pore ice surface and matrix was experimentally proved and is calculated according to Eq. (2c) proposed by Fagerlund [26].

It is well known that with the increase of concentration of chloride in water, the freezing temperature $T_0$ decreases. This is also valid for pore water. The equilibrium pore radius ($R_{peq}$) for water with different amount of chloride concentrations at a given temperature is calculated as [27]:

$$R_{peq} = R_{eq} + \delta, R_{eq} = \frac{2\tau\ cos\Theta\ V_c}{RT_f\ ln_{aw} - \mathrm{S_f}\,|\theta|}, \delta = 1.97|\theta|^{-\frac{1}{3}}, \theta = T_f - T_0 \quad (3)$$

where $R$ = gas constant (J/(K mol)); $V_c$ = molar volume of ice (m$^3$/mol), $ln_{aw}$ = activity of water in solution calculated from Fig. 1b; $S_f$ = molar fusion entropy (J/(K mol)). Parameters related to the calculation of equilibrium pore radius are shown in Table 1.

*Table 1: Input parameters for the calculation of equilibrium pore radius,R_peq*

| Property | Symbol | Units | Value |
|---|---|---|---|
| Surface tension of ice/water interface | $\tau$ | N/m | $\tau = (36 + 0.25\theta)x10^3$ |
| Mass density of water | $\rho_w$ | kg/m$^3$ | 1000 |
| Mass density of ice | $\rho_i$ | kg/m$^3$ | 917 |
| Fusion entropy density of ice | *Sf* | J/K x kg | $\frac{S_f}{V_c\ x\ \rho_i}$ |
| Molar fusion entropy of ice | $S_f$ | J/K x mol | 22 |
| Molar volume of ice | $V_c$ | m$^3$/mol | 0.0000196 |
| Contact angle | $\Theta$ | Degree (º) | Calculated based on chloride concentration in %, see Fig. 1a |
| Gas constant | *R* | J/K x mol | 8.31441 |
| Activity of water | $ln_{aw}$ | - | Calculated based on chloride concentration in mol, see Fig. 1b |
| Unfrozen layer thickness | $\delta$ | nm | $1.97\lvert\theta\rvert^{-\frac{1}{3}}$ |

The effect of chloride in the calculation of equilibrium pore radius is considered by including the contact angle and activity of water parameters, which are functions of salinity. Relationship between contact angle and chloride concentration (%) is shown in Fig. 1a [28]. For a given molality, the value of the activity of water can be calculated from the curve in Fig. 1b, which was provided by Lin and Lee [29].

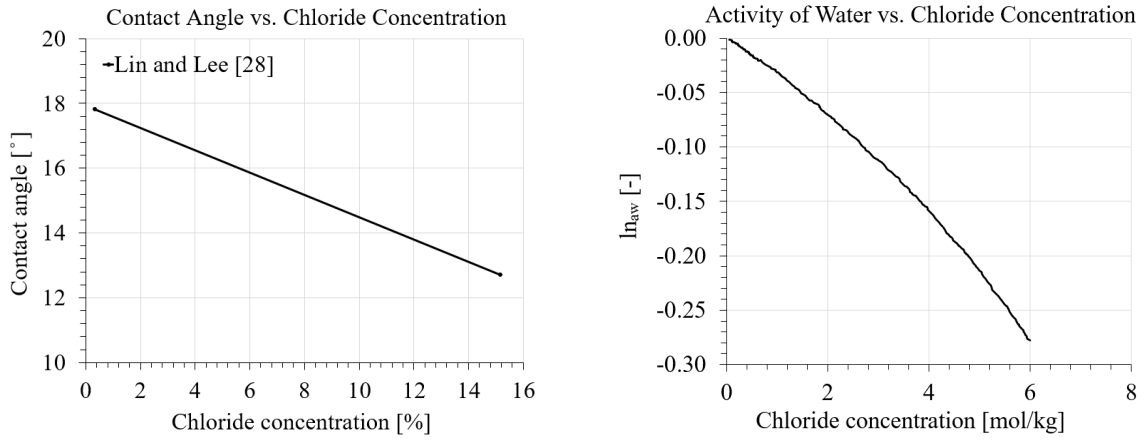


*(a)* *(b)*

*Fig. 1: Effect of chloride concentration on the equilibrium pore radius (a) relationship between chloride concentration and contact angle (b) relationship between chloride concentration and activity of water*

As can be seen from Figs. 1a and 1b, the value of chloride concentration for the calculation of contact angle and activity of water is introduced as percentage and

molality, respectively. Below relationship can be used to convert the concentration of chloride from percentage to molality:

$$chloride\ molality = \frac{mass\ of\ chloride\ (\frac{gr}{kg\ of\ water})}{molar\ mass\ of\ chloride\ (\frac{gr}{mol})} \qquad [\frac{mol}{kg\ of\ water}]$$

According to Eq. (2c) for pure water and Eq. (3) for water with different levels of chloride concentration, at a given temperature and molality, pores with an equilibrium pore radius larger than $R_{peq}$ should freeze, while those with a radius smaller than $R_{peq}$ should remain unfrozen. Based on these two equations, Fig. 2 depicts the development of the equilibrium pore radius of the porous medium (cement paste) with respect to the varying chloride concentrations and temperatures. It can be seen that the freezing temperature decreases as the pore radius becomes smaller and salinity of the water increases.

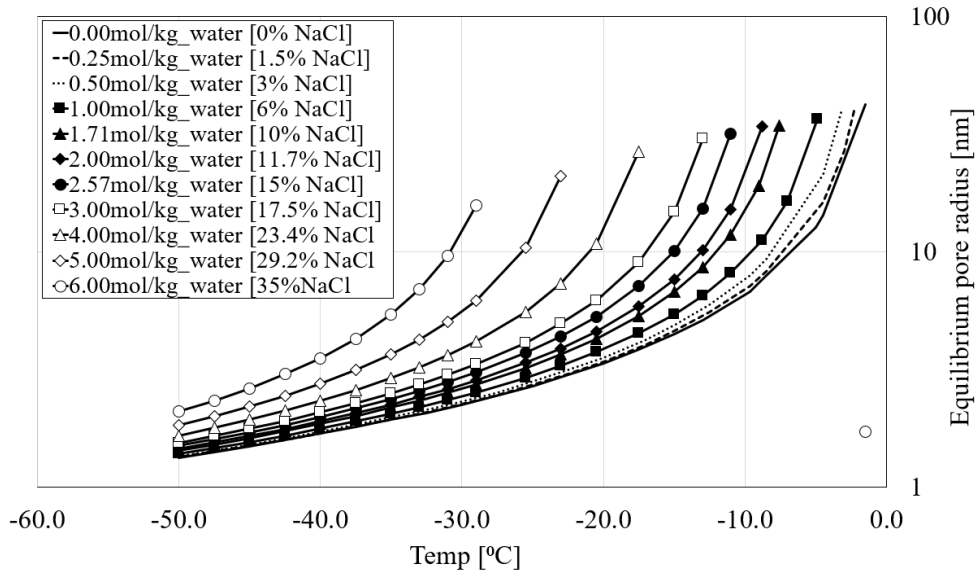


*Fig. 2: Evolution of equilibrium pore radius with varying chloride concentrations and temperature*

### *2.1.2 Effective pore pressure*

In Eq. (1), *S* denotes the source of pressure. It is composed of four terms. The first term corresponds to the pressures created by the formation of ice. The second term considers the pressure generated during temperature changes as a result of the difference between the thermal expansions of various phases. The last two terms correspond to the depression imposed on liquid water through the ice/water interface.

Based on the homogenization approach proposed in [25], the effective pore pressure $p^*$ of frozen continuum at the macro scale is calculated as:

$$p^* = p_w + X \tag{4}$$

where, as mentioned above, $X$ (Eq. 2d) is related to the pressure due to the presence of ice in the frozen pores, $p_w$ denotes liquid pressure. Note that $p^*$ (internal pore pressure) is responsible for the mechanical action and it comes into the equilibrium equation.

### 2.2 Energy Conservation Equation

The differential equation for heat conduction takes the following form [25]:

$$\rho C\dot{T} = \nabla \cdot (\lambda \nabla T) + L\,\dot{w}_i \tag{5}$$

$$\lambda = \frac{nS_w\lambda_w + nS_i\lambda_i + \lambda_m}{nS_w + nS_i + 1} \quad C = \frac{nS_wC_w + nS_iC_i + C_m}{nS_w + nS_i + 1}$$

where $\rho$ = density of the system (kg/m$^3$); $\lambda$ , $\lambda_w, \lambda_i, \lambda_m$ = thermal conductivity of the system, water, ice, and solid matrix respectively (W/(m K)); $C$ , $C_w, C_i, C_m$ = heat capacity of the system, water, ice and solid matrix respectively (J/(kg K)) and $L$ = latent heat of fusion of water (kJ/kg). The last term in Eq. (5) introduces a coupling between the heat transfer and the phase change and has an appreciable effect in freeze-thaw problems.

### 2.3 Momentum Equation

The governing equation for the mechanical behavior of a continuous body in case of static loading condition reads:

$$\nabla(C_m\nabla u) - \nabla p_T - b\nabla p^* + f = 0 \tag{6}$$

where $C_m$ = material stiffness tensor; $u$ = displacement field; $p_T$ = volumetric stress due to free thermal strains of the porous material; $f$ = specific volume load.

## 3. VERIFICATION OF THE MODEL: 3D FINITE ELEMENT ANALYSIS

To solve the above partial differential equations by using finite elements, the strong form of the formulation (Eqs. 1, 5 and 6) is first rewritten into a weak form [30]. The weak form of the system of partial differential equations is based on the

Galerkin weighted residual method. The model is then implemented into a 3D FE code. The non-mechanical part of the problem (Eqs. 1 and 2) is solved iteratively by using direct integration method of implicit type [31]. To solve the mechanical part (Eq. 6), Newton-Rapshon iterative scheme is used. The coupling between mechanical and non-mechanical part of the model is per-formed by continuous update of governing parameters during the incremental transient finite element analysis using staggered solution scheme. The analysis is performed assuming saturated continuum and linear elasticity.

### *3.1 Geometry and FE discretization*

The present numerical study is carried out based on the experimental and numerical work of Zeng et al. [8] on the freezing behavior of cement paste saturated with different chloride concentrations. The cylindrical specimens have a diameter of 10 mm and a height of 100 mm. In their original work, two different cement pastes with water-cement ratios of 0.50 and 0.30 and six different chloride concentrations were investigated numerically and experimentally. The experimental results reported in [8] include four freeze-thaw cycles. The results, based on the poroelastic model proposed in [8], show fairly good agreement with the experimental tests for the first cooling phase.

In the present study, the cylinders with two cement pastes investigated in [8] were numerically analyzed to reproduce the freezing behavior of the material when saturated with different chloride concentrations. The water-cement ratio, boundary conditions and freezing rate were set as given in [8] (see Table 2). As in the experimental tests, cement pastes with water-cement ratios of 0.50 (PI) and 0.30 (PII) were investigated. The results from [8] were used to verify the numerical model.

The FE discretization was performed using 1600 solid eight-node elements with an average element size of 2 mm. (Fig. 3a). The mechanical and environmental boundary conditions of the FE model are shown in Figs. 3a and 3b. Based on the information provided in [8], the specimens were kept vertically inside the environmental chamber with all free surfaces. Therefore, a simply supported constraint was applied to the bottom surface of the model (see Fig. 3a). During the freezing test in [8], the temperature variation was applied through the environmental chamber to all surfaces of the specimens with the same freezing rate, as illustrated in Fig. 4. The freezing rate for the first cooling phase was 20°C/h which

lasted for 2.75 hours. The hydraulic pore pressure at the surface of the specimen and the initial hydraulic pressure was set to zero, e.g. approximately atmospheric pressure (0.10 MPa).

The same as in [8], the environmental boundary conditions were applied to all external surfaces of the model as heat flux (Fig. 3b). Time step for the numerical simulation was set to 150s throughout the freezing phase. The first cooling phase of the simulation is consisting of 66-time steps corresponding to 2.75 hours.

*Table 2: Two simulation cases*

| Case | Water/cement ratio | Size (mm) | Chloride concentration (%) | Freezing rate and temperature range |
|---|---|---|---|---|
| 1 | 0.50 | 10 x 100 cylinder | 0, 1.5, 3, 6, 10, 15 | Fig. 4 |
| 2 | 0.30 | 10 x 100 cylinder | 0, 1.5, 3, 6, 10, 15 | Fig. 4 |

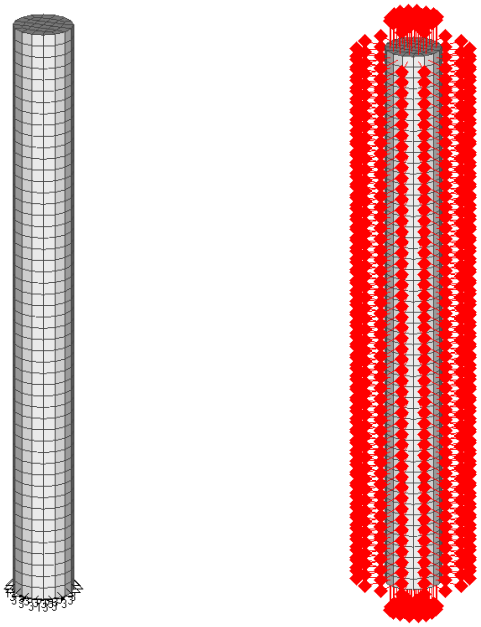

*(a)* *(b)*

*Fig. 3: FE model, (a) mechanical boundary condition (b) environmental boundary condition*

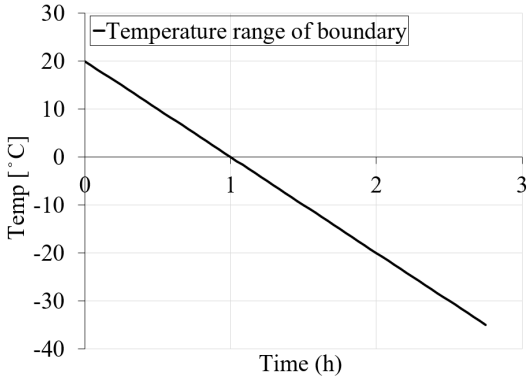


*Fig. 4: Temperature-time variation for the first cooling phase*

### 3.2 Material Parameters

The input parameters of the porous medium and solid skeleton for PI (PII) cement pastes are summarized in Table 3. Water/cement ratio, total porosity, compressibility modulus of the porous skeleton and compressibility modulus of solid matrix were provided in [8]. Biot's coefficient is calculated as:

$$b = 1 - \frac{K_0}{K_m} \tag{7}$$

where $K_0$ is the compressibility modulus of the porous skeleton and $K_m$ is the compressibility modulus of the solid matrix. The elastic modulus and liquid water permeability of PI and PII are calculated based on Eq. 8. and Eq. 9, respectively. The Poisson's ratio, thermal conductivity and heat capacity of the cement pastes are extracted from the literature.

*Table 3: Input material properties of porous medium and solid skeleton for PI (PII) cement pastes*

| Property | Symbol | Units | Value |
|---|---|---|---|
| Apparent density | $\rho$ | (g/ml) | 1.6 (2) |
| Poisson's ratio | $v$ | - | 0.20 |
| Water-cement ratio | - | - | 0.50 (0.30) |
| Total porosity | $n$ | ($m^3/m^3$) | 0.26 (0.13) Fig. 5 |
| Elastic modulus | $E$ | (GPa) | 26 (36)<br>$E = 3(K_0)(1-2v)$ |
| Compressibility modulus of the porous skeleton | $K_0$ | (GPa) | 14.6 (20.2)<br>$K_0 = E/3(1-2v)$ |
| Compressibility modulus of the solid matrix | $K_m$ | (GPa) | 31.8<br>$K_m = K_0/(1-n)^3$ |
| Biot's coefficient | $b$ | - | $b = 1-K_0/K_m$ |
| Pore size distribution | - | (% by vol) | Fig. 5 |
| Thermal conductivity | $\lambda_m$ | [W/(m x K)] | 1.15 (1.35) |
| Heat capacity | $C_m$ | [J/kg x K] | 850.0 |
| Thermal expansion coefficient | $\alpha$ | $^{\circ}C^{-1}$ | $1.20 \times 10^{-5}$ ($1.86 \times 10^{-5}$) |
| Liquid water permeability | $D$ | ($m^2$) | $2.78 \times 10^{-21}$ ($2.29 \times 10^{-19}$) |

The elastic modulus of PI and PII cement pastes listed in Table 3 were not directly provided in [8], however, in the current model it is calculated based on the Eq. 8, which sets relationship between the compressibility modulus of the porous skeleton ($K_0$) and Poisson's ratio ($v$).

$$K_0 = \frac{E}{3(1-2v)} \tag{8}$$

The parameter of liquid water permeability was also not provided in the poroelastic model from [8] because it was assumed that the freezing can instantaneously occur to the entire sample due to its small size. Here the value of the liquid water permeability for PI and PII is calculated based on the total porosity using the formula provided by Powers in [2]. The relationship from [2] is modified with one smaller order of magnitude such that the freezing strains best fit the experimental and numerical results in [8]. The final relationship between liquid water permeability and porosity is taken as (Eq. 9):

$$D = 3.55(n^{3.6})10^{-19}[\mathrm{m}^2] \tag{9}$$

where $n$ is the total porosity.

The thermal expansion coefficient values for two different cement pastes (PI and PII) were calculated based on the total porosity of the cement paste provided in [8] as (Eq. 10):

$$\alpha_d = \alpha_c(1-n)^{2.66} \text{ [33]} \tag{10}$$

with $\alpha_c = 26.98 \text{ x } 10^{-6} /^{\circ}C$ .

Table 4 presents the input material properties for water and ice. The compressibility of water and ice is given by Zuber et al. [14]. Density, heat capacity and thermal conductivity for water and ice are being extracted from [14] and [25]. The dynamic viscosity of water is given in [25].

*Table 4: Input material properties of water and ice*

| Property | Symbol | Units | Value |
|---|---|---|---|
| Density of water | $\rho_w$ | (g/cm$^3$) | 1.0 |
| Water compressibility | $K_w$ | (GPa) | 2 |
| Liquid water coefficient of volumetric thermal expansion | $\alpha_l$ | [°C$^{-1}$] | $\alpha_l = (-9.2+2.07\Theta)\ x10^{-5}$ |
| Thermal conductivity of water | $\lambda_w$ | [W/(m x K)] | 0.55 |
| Heat capacity of water | $C_w$ | [J/(g x K)] | 4.22 |
| Dynamic viscosity of water | $\eta$ | (Pa × s) | $\eta = 1.38 \times 10^{-6}$ $exp(2.590/T)$ with $T$ in K |
| Density of ice | $\rho_i$ | (g/cm$^3$) | 0.916 |
| Ice compressibility | $K_i$ | (GPa) | 8 |
| Ice coefficient of volumetric thermal expansion | $\alpha_i$ | [°C$^{-1}$] | $\alpha_i = 5.5(1+ (\Theta/200))\ x\ 10^{-5}$ |
| Thermal conductivity of ice | $\lambda_i$ | [W/(m x K)] | 2.20 |
| Heat capacity of ice | $C_i$ | [J/(g x K)] | 2.11 |

## 3.3 Pore size distribution

The pore size distribution (PSD) curves used in the model are taken from [8]. The curves were experimentally obtained for PI and PII cement pastes through the mercury intrusion porosimetry (MIP) method. Fig. 5 shows the obtained pore size distribution curves.

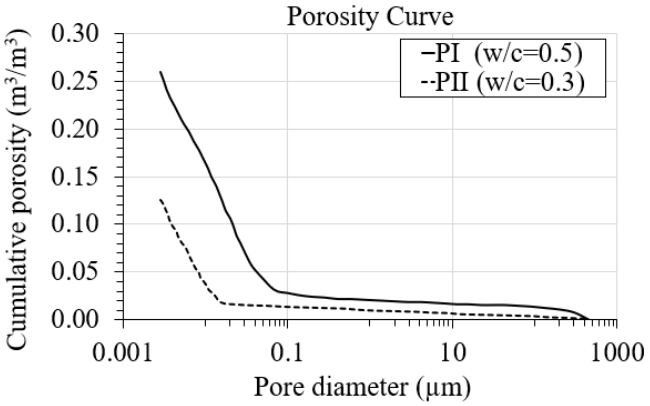


*Fig. 5: Pore size distribution of PI and PII cement pastes*

## 3.4 Numerical results and discussion

### 3.4.1 PI Cement Paste (0.50 w/c ratio)

#### Freezing strains

As previously discussed, Zeng et al. [8] performed experimental and numerical study on two cement pastes with water-cement ratio of 0.50 (PI) and 0.30 (PII), respectively. The authors analysed the cylindrical specimen (height = 100 mm, diameter = 10 mm) saturated with different chloride concentrations: 0, 1.5, 3, 6, 10 and 15 %. The experimental results showed that the ice saturation degree was influenced by both porosity and pore connectivity of the two different pastes.

Similar to the experimental and numerical work presented in [8], in the present study, the first set of simulations for PI with a water-cement ratio of 0.50 (case 1) and chloride concentrations of 0, 1.5, 3, 6, 10 and 15 % were simulated for the first cooling phase ranging from +20 to -35°C, as shown in Fig. 4. The results in terms of average axial strains were compared with the experimental and numerical curves reported in [8] and shown in Fig. 6.

As can be seen from Fig. 6, the results obtained in the present numerical study agree well with the numerical results obtained in [8]. Comparing the numerical curves, a transition between the contraction phase and the expansion phase in terms of the average uniaxial strain can be observed in all cases. In particular, the transition point decreases as the amount of chloride increases. This is consistent with the equilibrium pore radius curves shown in Fig. 2. Fig. 6 shows that with increasing chloride concentration, the freezing point of the solution is shifted, resulting in less freezing strain.

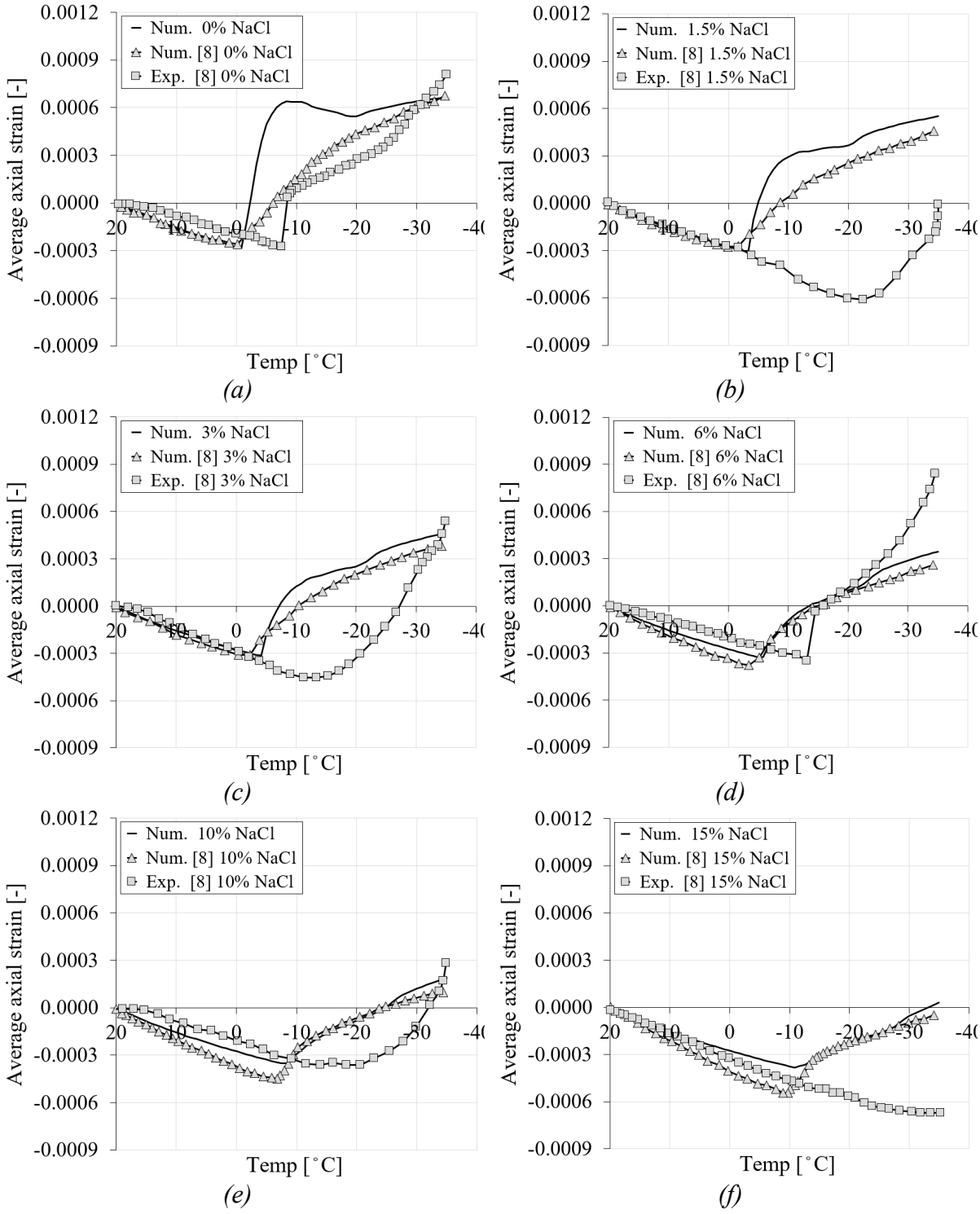


*Fig. 6: The comparison between the freezing strains of the current study and experimental and numerical results from [8] for PI cement paste during the first cooling phase (a) pure water (b) 1.5 % NaCl (c) 3 % NaCl (d) 6 % NaCl (e) 10 % NaCl (f) 15 % NaCl*

## *Pore pressure*

The pore pressure of porous media, as the sum of hydraulic and ice pressure, is directly related to the size and structure of the pores. In fully-saturated conditions, an increase in the porosity of the material leads to more freezing, with consequent

higher pore pressure and deformation. To observe the ice, liquid and pore pressure during the freezing process, seven nodes were selected across the mid-height of the specimen (see Fig. 7). The evolution of the pore pressure with temperature is shown in Fig. 8. Due to the symmetry, the results are shown only for nodes 1038, 1041, 1043 and 1045. Fig. 8a shows comparison between the pore pressure of the selected nodes with respect to their locations within the specimen for pure water. The results show that by moving towards the surface of the specimen, the pore pressure reduces. Based on the cooling regime, negative pore pressure due to the thermal contraction of the pore solution can be observed until the temperature reaches the freezing point of the pore solution. However, after the temperature goes below the freezing point of the solution, due to freezing inside the pores, positive pore pressure develops. This pore pressure is consistent with the freezing induced expansion of the specimen.

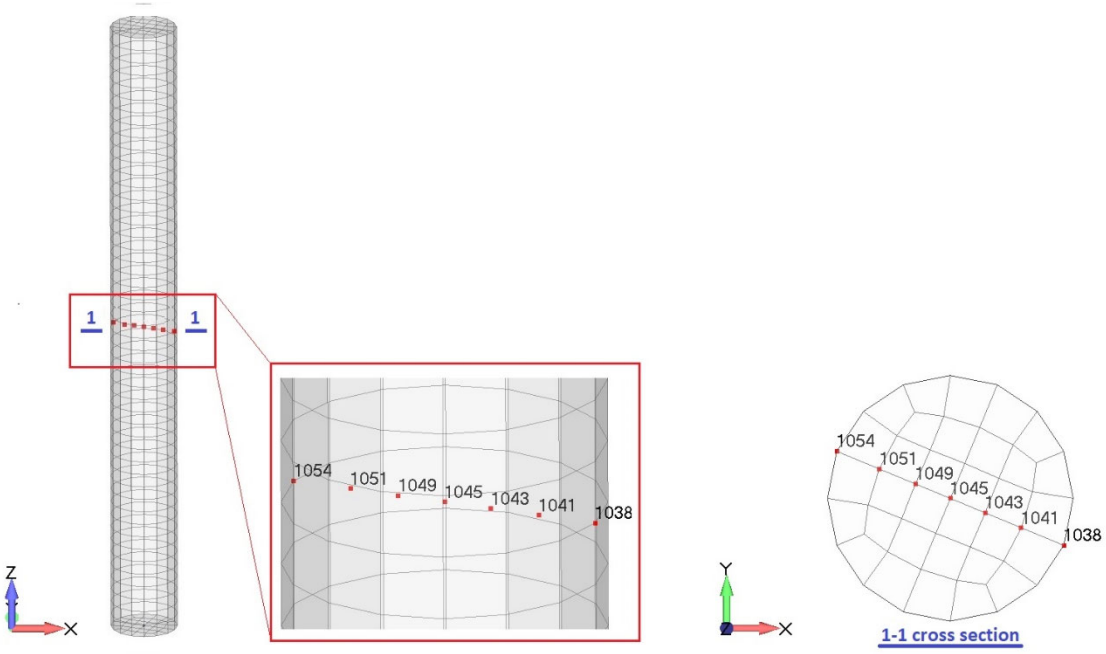


*Fig. 7: Arbitrary nodes for freezing induced liquid, ice and pore pressure*

Figs. 8b to 8d show the pore pressure results of the same nodes for 3, 6 and 15 % of chloride concentrations. It can be seen that by increasing the amount of chloride, the pore pressure reduces. This is mainly related to the fact that the freezing temperature of the solution decreases with increasing chloride concentration. Additionally, the transition point shifts towards the negative temperature as the amount of chloride increases (Fig. 8).

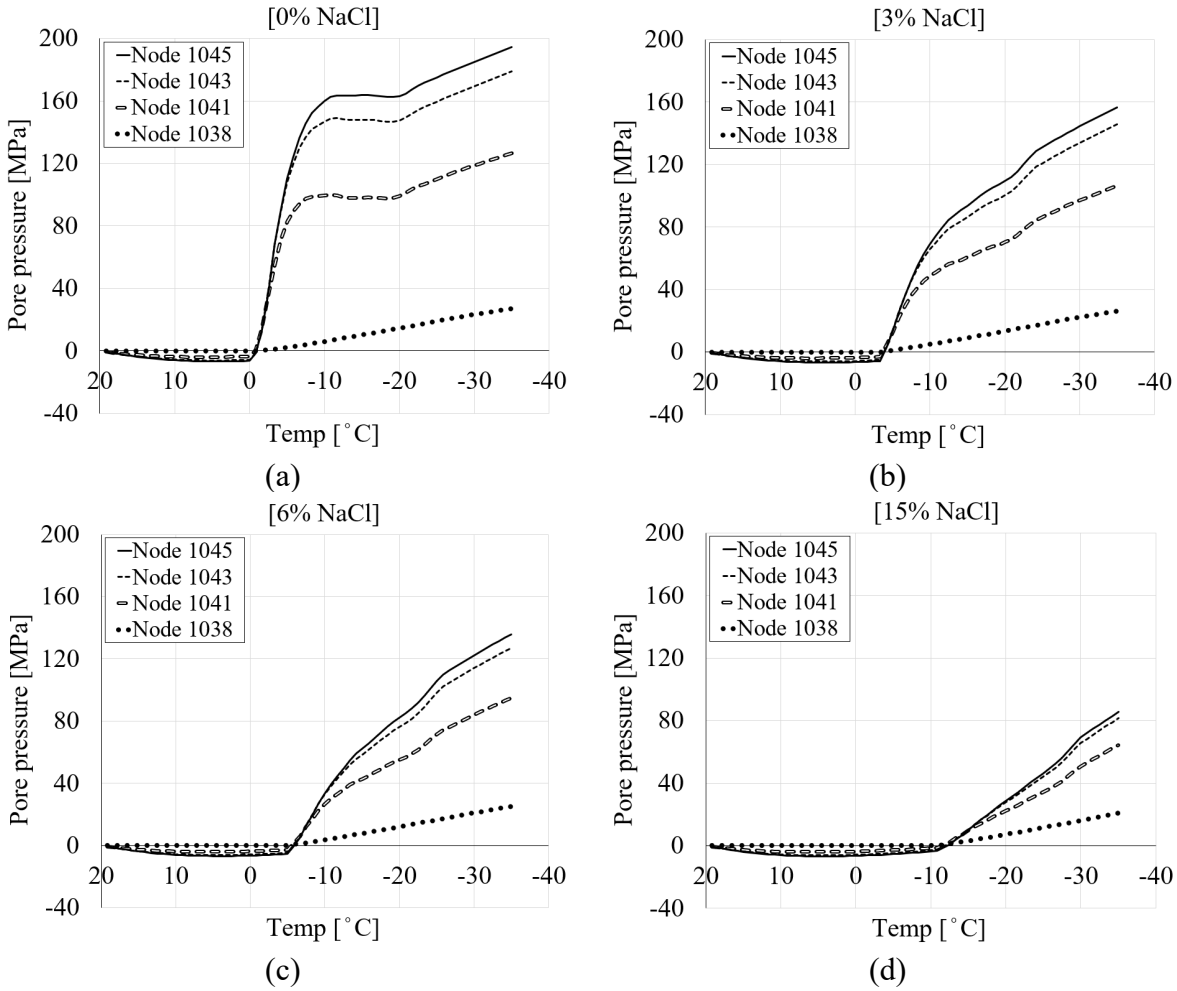


*Fig. 8: The comparison between the pore pressure of four selected nodes for PI cement paste during the first cooling phase with respect to temperature variation (a) pure water (b) 3 % NaCl (c) 6 % NaCl (d) 15 % NaCl*

Fig. 9 shows the spatial distribution of the pore pressure for the selected seven nodes (see Fig. 7) during the first cooling phase. The pore pressure variation versus the distance of the nodes from the center of the specimen is shown for (i) six different chloride concentrations and (ii) nine time steps of the analysis. Each point on the curves corresponds to one selected node. The first step (S1≈ 19.2℃) corresponds to the beginning of the cooling phase, while the last one (S66≈ -35℃) refers to the end of the cooling phase.

Figs. 9b to 9d show the same results for 3, 6, and 15 % chloride concentrations. It is clear from Fig. 9b (3 % NaCl) that the pore pressure of the corresponding time steps compared to 0 % chloride concentration is smaller due to the delay in the freezing of solution inside the pores as a result of chloride concentration.

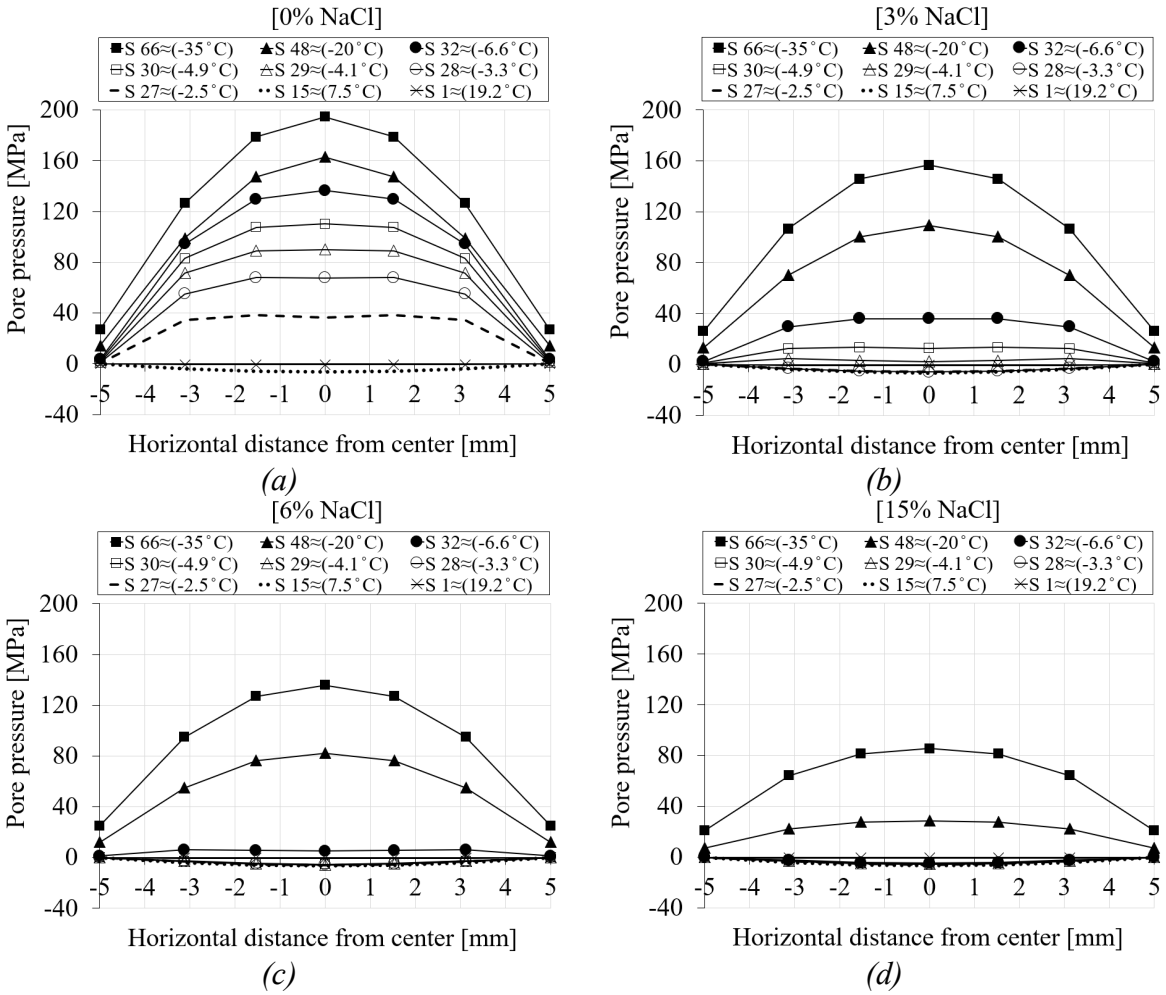


*Fig. 9: The comparison between the pore pressure of the seven selected nodes in terms of distance and time step for PI cement paste during the first cooling phase (a) pure water (b) 3 % NaCl (c) 6 % NaCl (d) 15 % NaCl*

## *Ice pressure*

Fig. 10 shows the contribution of the ice pressure during the freezing process for two levels of chloride concentrations, namely pure water and 15 % chloride. It only depicts the ice pressure once the temperature goes below the freezing point of the solution. It is visible from the curves in Fig. 10 that the ice pressure is zero until solution inside the pores starts freezing.

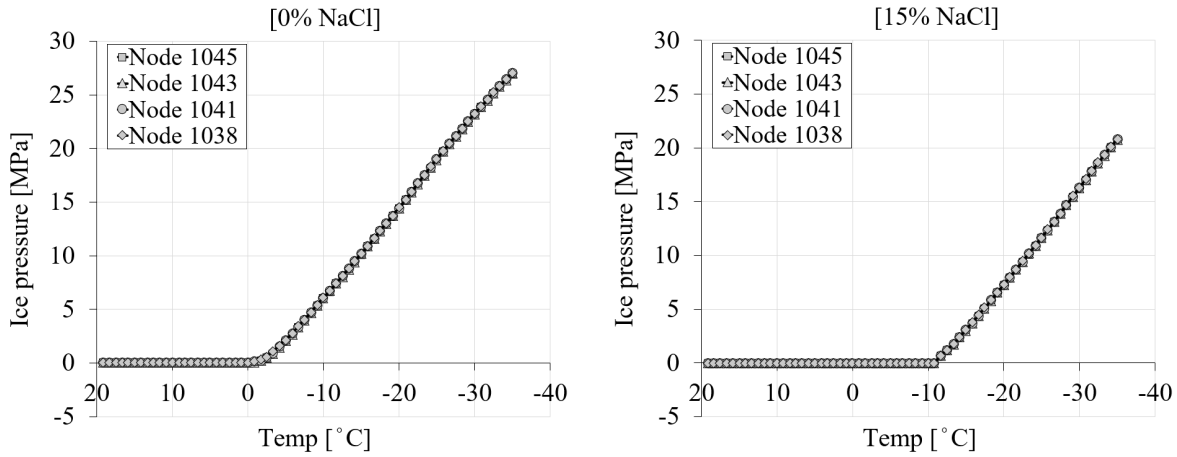


*Fig. 10: The comparison between the ice pressure of four selected nodes for PI cement paste during the first cooling phase with respect to temperature variation (a) pure, (b) 15 % NaCl*

Fig. 11 represents the ice pressure in terms of freezing time and distance of the nodes from the center of the specimen for two specified chloride concentrations (see Fig. 7) during the first cooling phase.

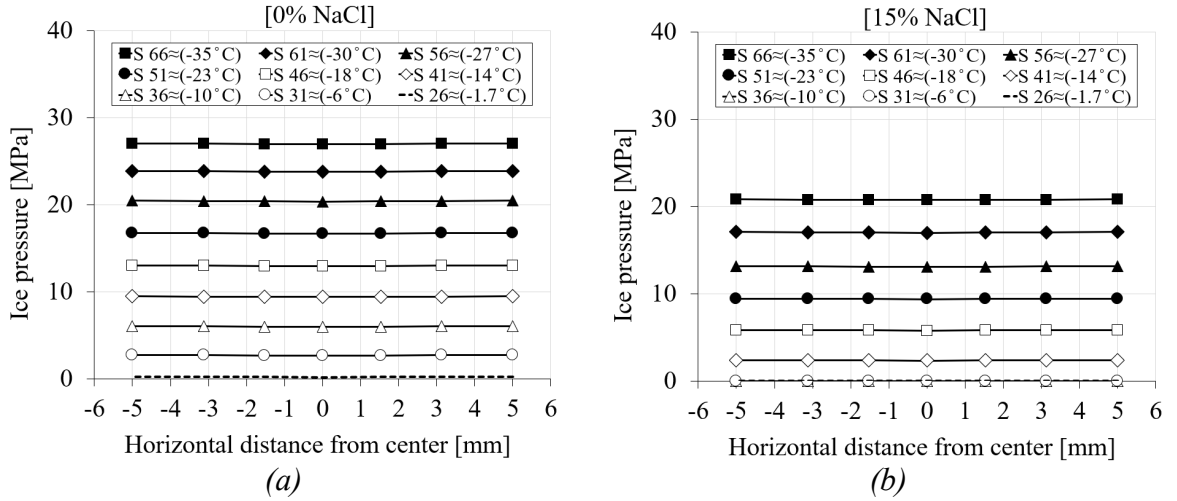


*Fig. 11: The comparison between the ice pressure of the seven selected nodes in terms of distance and time step for PI cement paste during the first cooling phase (a) pure water (b) 15 % NaCl*

## *Liquid [hydraulic] pressure*

The liquid pressure inside the pores is an important source of freezing deformation in the porous media. Liquid pressure generates as a result of the viscous flow of water into the pore spaces in an undrained or low permeability condition. According to [34], liquid pressure inside the pores may reach a magnitude of 150 MPa. Liquid pressure together with ice pressure forms pore pressure which is the main source of freezing stress and deformation in porous material. Fig. 12 shows the

liquid pressure of the selected four nodes for pure water and 15 % chloride concentration during the cooling phase.

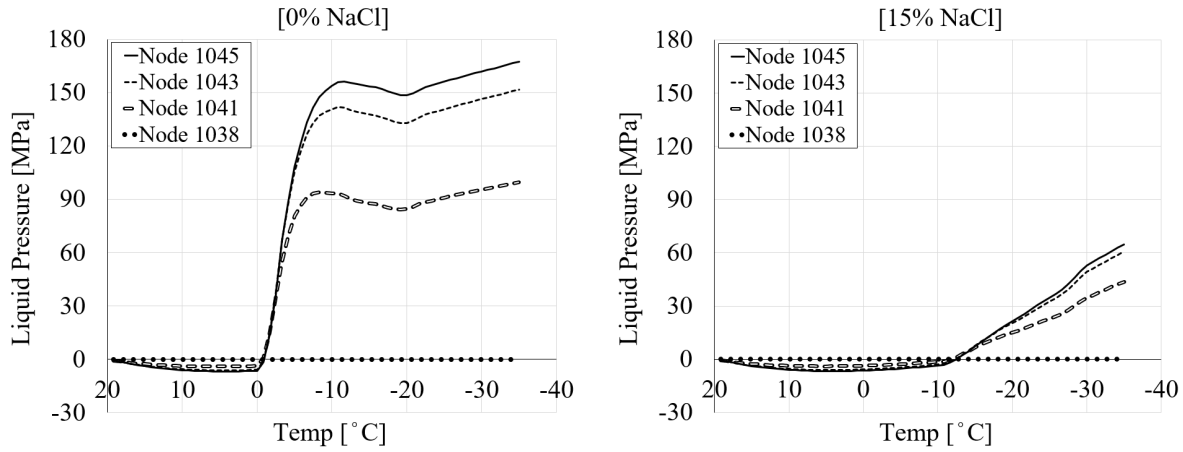


*(a)* *(b)*

*Fig. 12: The comparison between the liquid pressure of four selected nodes for PI cement paste during the first cooling phase with respect to temperature variation (a) pure, (b) 15 % NaCl*

To better visualize how the liquid pressure changes across the section of the specimen, Fig. 13 shows the spatial representation of the liquid pressure for seven selected nodes and two chloride concentrations during the cooling phases.

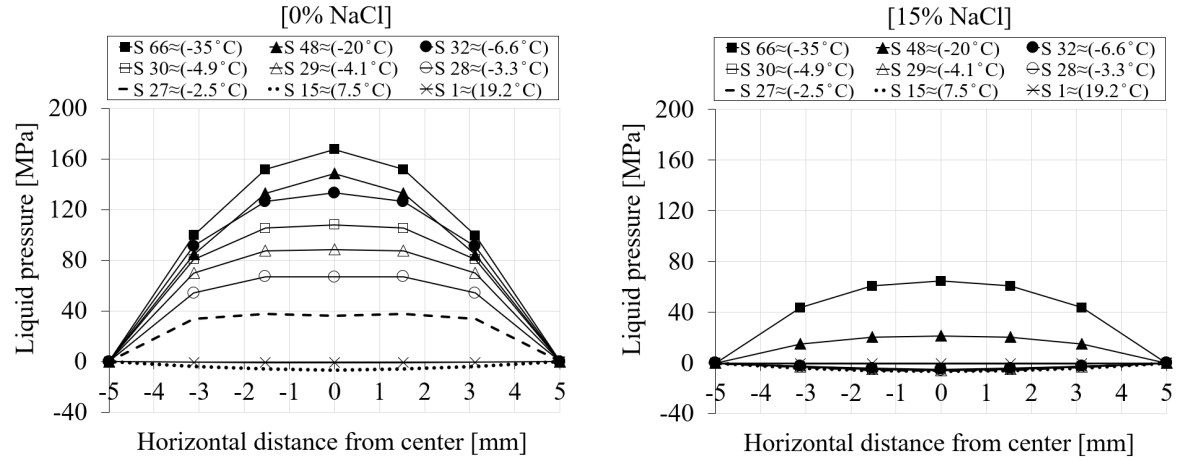


*(a)* *(b)*

*Fig. 13: The comparison between the liquid pressure of the seven selected nodes in terms of distance and time step for PI cement paste during the first cooling phase (a) pure water (b) 15 % NaCl*

### *Influence of the freezing point on the freezing process*

To this end, the numerical results shown for PI cement pastes were based on the development of the equilibrium pore radius with varying chloride concentrations and temperature according to Fig. 2. The average axial strain for PI cement paste reported in Fig. 6 were in reasonable agreement with the numerical results in [8].

However, if a comparison is carried out between the numerical and experimental results in [8], it can be seen that for the experimental curves, there is a delay in the freezing process and freezing point of the pore solution. Considering that (i) experimentally it takes slightly longer for the freezing process to occur after the temperature (cooling) is applied, and (ii) the degree of saturation of the pores affects the freezing-induced strains, the freezing points of the pore solution, as indicated in Fig. 2 for the calculation of the equilibrium pore radius, were modified in the model to correspond to the points observed in the experiments [8].

Fig. 14 shows the average axial strain of PI cement paste for 0 % and 3 % chloride concentrations with the original and modified freezing point of the pore solution and their comparison with the results from [8]. The dotted line shows the average axial strain of the current study where the freezing point of the solution was controlled based on the equilibrium pore radius in Fig. 2. However, the solid line shows the same results with the modified freezing point according to the experimental results [8]. It can be seen that a delay in the freezing process of the pore solution has significant influence on the resulting average axial strain (Fig. 14). The new numerical results for two chloride cases show a very good agreement with the experimental results from [8].

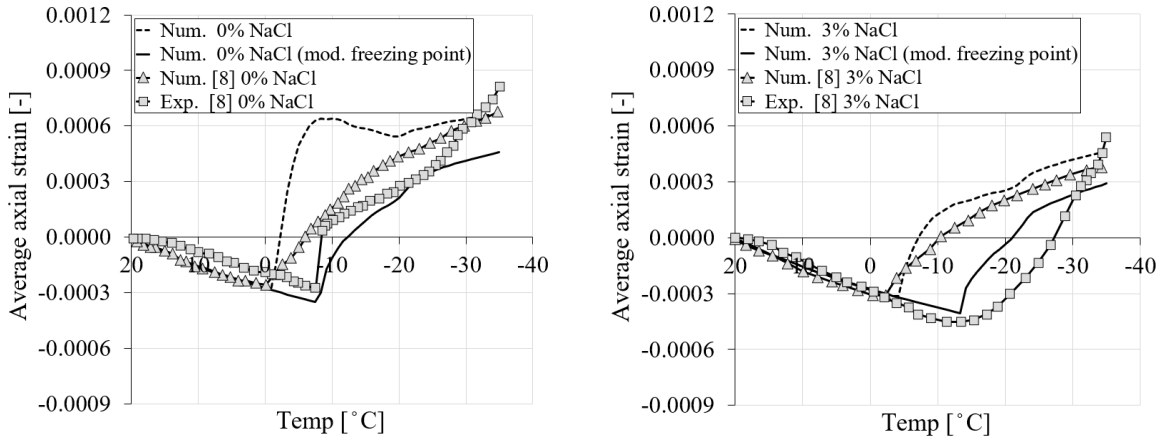


*Fig. 14: The comparison between the average axial strain of the modified and original freezing point of the present model with the numerical and experimental results in [8] in terms of freezing temperature for PI cement paste during the first cooling phase (a) 0 % NaCl (b) 3 % NaCl*

To investigate the effect of the delayed freezing temperature on the pore pressure of PI cement paste, Fig. 15 shows the pore pressure for 0 % chloride concentration, obtained with two different freezing point, i.e., -9°C in Fig. 15a and -0.1°C in Fig. 15b. It is obvious from Fig. 15a that by decreasing the freezing point of

the pore solution, the freezing process delays and consequently results in lower pore pressure which is the main source of deformation.

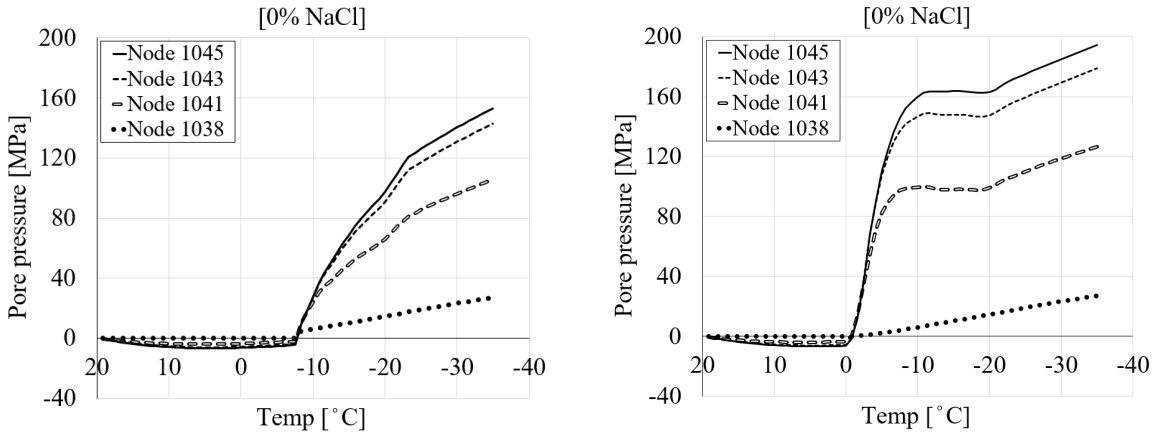


*Fig. 15: The comparison between the pore pressure of the modified and original freezing point of the present model in terms of freezing temperature for PI cement paste during the first cooling phase (a) freezing point -9°C and (b) freezing point -0.1°C*

To better clarify how the pore pressure distribution across the section is affected by the delay in the freezing process, spatial representation of the results is shown in Fig. 16 for 0 % chloride concentration and two different freezing points, i.e. -9°C in Fig. 16a and -0.1°C in Fig. 16b.

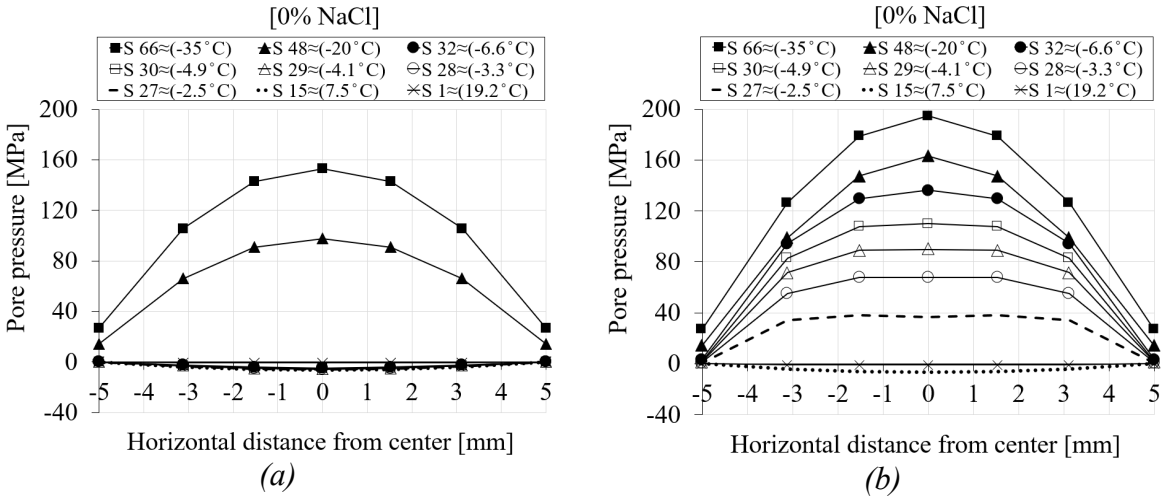


*Fig 16: The comparison between the pore pressure results of the modified and original freezing point of the present model in terms of distance for PI cement paste during the first cooling phase (a) freezing point -9°C and (b) freezing point -0.1°C*

### *3.4.2 PII Cement Paste (0.30 w/c ratio)*

The second set of simulations for PII cement paste with a water-cement ratio of 0.30 (case 2) and chloride concentrations of 0, 3, 6, and 15 % were simulated and

the resultant average axial strains were compared to that of the experimental and numerical results from [8]. The results are shown in Fig. 17.

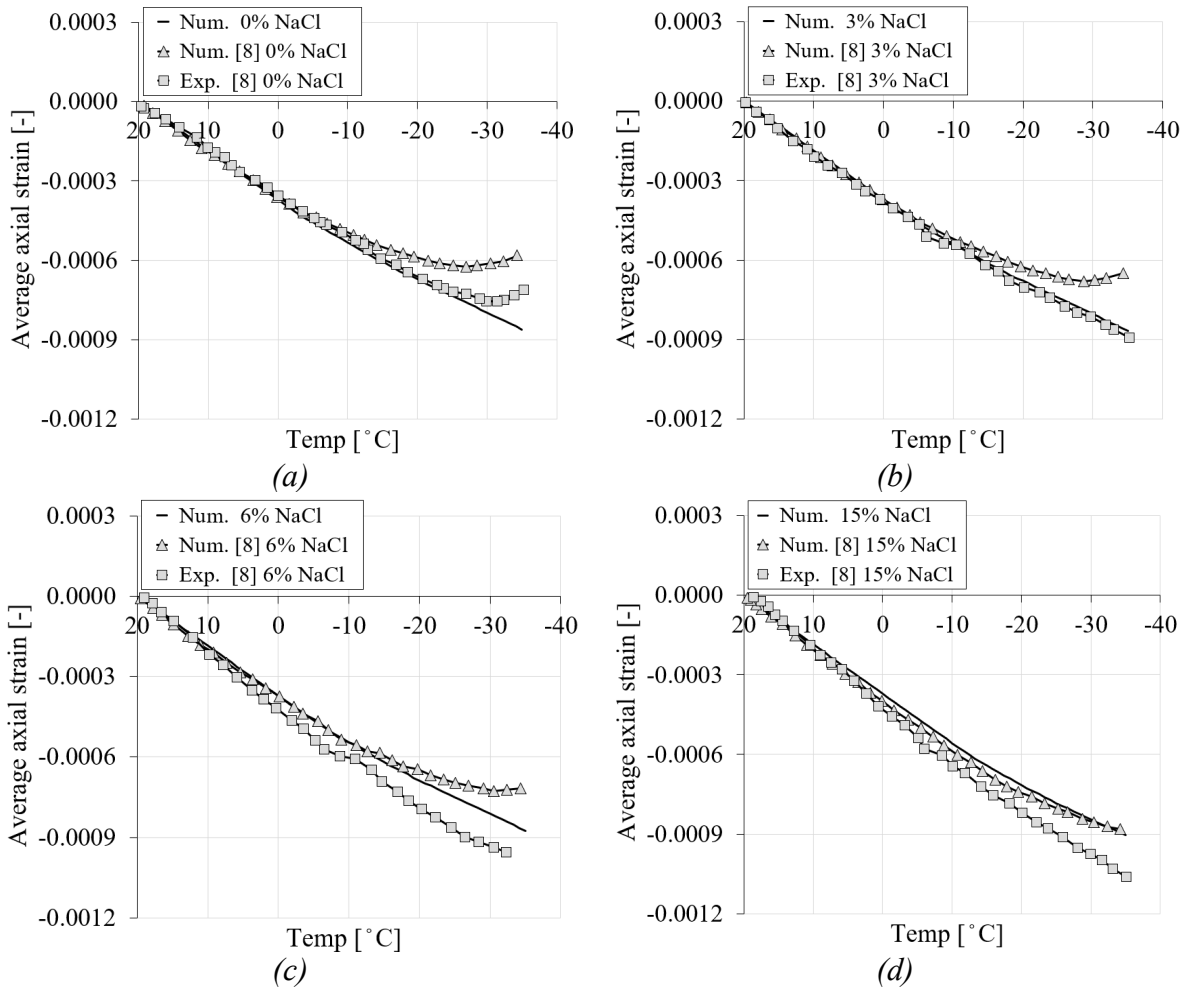


*Fig. 17: The comparison between the freezing strains of the current study and experimental and numerical results in [8] for PII cement paste during the first cooling phase (a) pure water (b) 3 % NaCl (c) 6 % NaCl (d) 15 % NaCl*

As can be seen, the experimental and numerical results for PII specimens from [8] show very different deformation response compared to the PI specimens. All specimens showed no visible expansion at below-freezing temperatures and no appreciable residual freezing strain. The denser microstructure of PII material compared to PI cement paste can be the only reason for this difference. The paste includes much fewer capillary pores and has substantially less pore percolation due to its lower w/c ratio of 0.30.

# 4. PARAMETRIC STUDY

After the validation of the 3D FE model, a parametric study was performed on PI cement paste to investigate the influence of liquid water permeability, total porosity and pore size distribution on the average axial strain and generated ice and pore pressure for the first cooling phase. The parametric study was performed by for two cases as shown in Table 5.

*Table 5: Parametric study values for PI cement paste*

| | **Liquid water permeability ($m^2$) (Ref. value 2.78 x $10^{-21}$ $m^2$)** | **Total porosity** | **Pore size distribution** |
|---|---|---|---|
| **CASE 1** | 6.95 x $10^{-22}$ (–25 % of Ref. value) | 0.26 | (1) in Fig. 18 |
| | 3.48 x $10^{-21}$(+25 % of Ref. value) | 0.26 | (1) in Fig. 18 |
| | 1.39 x $10^{-21}$ (–50 % of Ref. value) | 0.26 | (1) in Fig. 18 |
| | 4.17 x $10^{-21}$ (+50 % of Ref. value) | 0.26 | (1) in Fig. 18 |
| | 2.09 x $10^{-21}$ (–75 % of Ref. value) | 0.26 | (1) in Fig. 18 |
| | 4.87 x $10^{-21}$ (+75 % of Ref. value) | 0.26 | (1) in Fig. 18 |
| **CASE 2** | Total porosity (Ref. Value 0.26) | Liquid water permeability ($m^2$) | Pore size distribution |
| | 0.22 (85 % of Ref. value) | 1.52 x $10^{-21}$ | (2) in Fig. 18 |
| | 0.18 (70 % of Ref. value) | 7.40 x $10^{-22}$ | (3) in Fig. 18 |
| | 0.14 (55 % of Ref. value) | 2.99 x $10^{-22}$ | (4) in Fig. 18 |

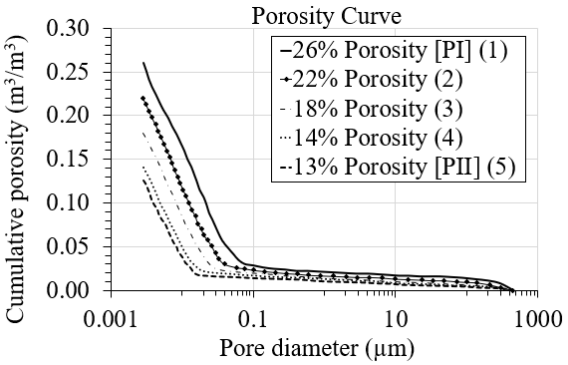


*Fig. 18: Pore size distribution for different porosity cases*

## *4.1 Case 1: Varying liquid water permeability*

In this series of studies, the influence of liquid water permeability compared to the calibrated (reference) value on the strain development and pore pressure of PI cement paste is investigated. The other material properties, including elastic modulus and boundary conditions are kept unchanged. The numerical results are shown in Fig. 19.

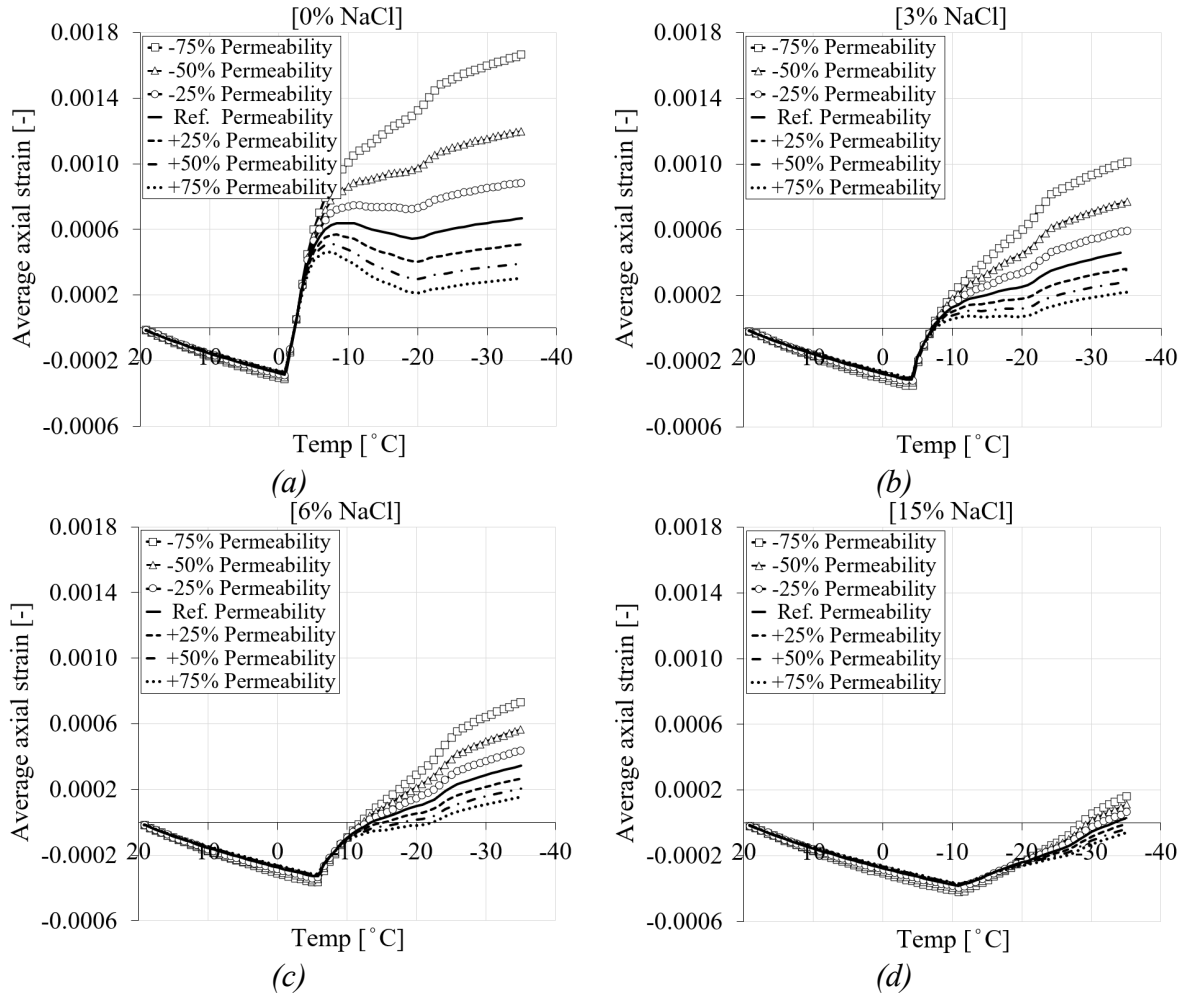


*Fig. 19: The comparison between the freezing strains of the reference liquid water permeability and six selected values based on Table 5 for PI cement paste during the first cooling phase (a) pure water (b) 3 % NaCl (c) 6 % NaCl (d) 15 % NaCl*

To better illustrate how changes in liquid water permeability affect the induced pore and ice pressure, pore and ice pressure for the first cooling phase are shown as a function of freezing time and distance in Fig. 20. Only the results for two extreme values of liquid water permeability compared to the reference value for 0 % chloride concentration are shown.

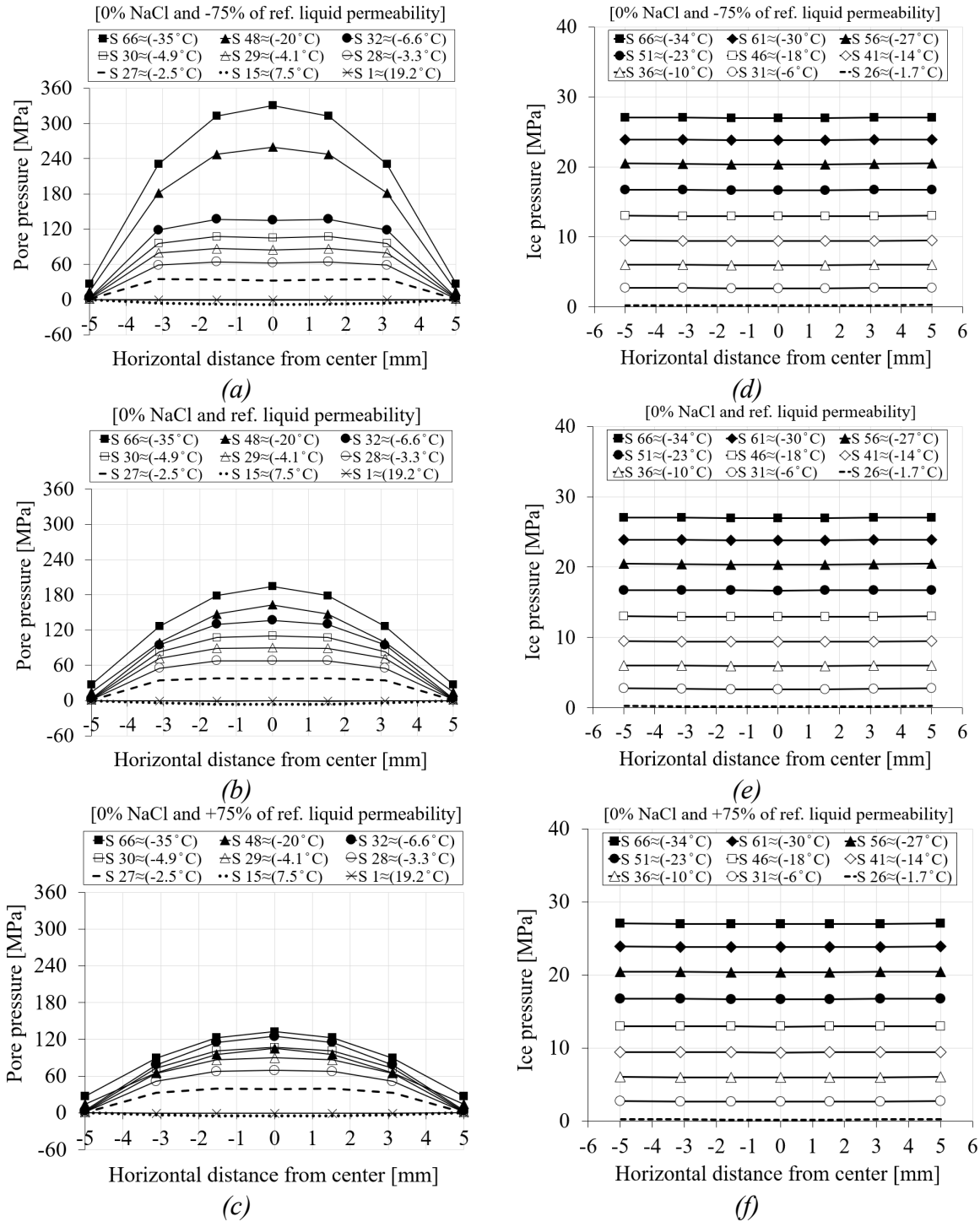


*Fig. 20: The comparison of the pore and ice pressure of seven selected nodes in terms of distance and time step between the reference and the two extreme liquid water permeability values for PI cement paste with 0 % chloride concentration during the first cooling phase, (a) to (c) pore pressure, (d) to (f) ice pressure*

## 4.2 Case 2: Varying liquid water permeability, total porosity and pore size distribution

This parametric study was performed to investigate the effect of simultaneous variations of liquid water permeability, total porosity and pore size distribution on the freezing strain and pore pressure of PI cement paste compared to the reference case.

Table 5 shows the three different values of total porosity and their corresponding liquid water permeability values used in this study. It should be noted that the coefficient of thermal expansion as a function of porosity is calculated for each porosity case based on Eq. 10 and reported in Table. 6.

*Table 6: Thermal expansion coefficient for four different porosity cases*

| **Total porosity** | **26 % (ref. value)** | **22 %** | **18 %** | **14 %** |
|---|---|---|---|---|
| Thermal expansion coefficient ($^{\circ}C^{-1}$) | $1.20 \times 10^{-5}$ (ref. value) | $1.39 \times 10^{-5}$ | $1.59 \times 10^{-5}$ | $1.81 \times 10^{-5}$ |

The numerical results showed that the influence of porosity and liquid water permeability can significantly affect the freezing strain of PI cement paste during the initial cooling stage. A comparison between the freezing strains of the reference case (reference liquid water permeability) and three selected values of porosity and liquid water permeability (Table 5) for four chloride concentrations is shown in Fig. 21.

In general, it can be seen that when the total porosity is decreased, the material becomes denser and contracts more due to the effect of thermal expansion coefficient under decreasing temperature. Consequently, the freezing strain will decrease. The results show that the material with smaller total porosity contracts more and therefore its induced freezing strain (expansion) is smaller than in the case of higher porosity.

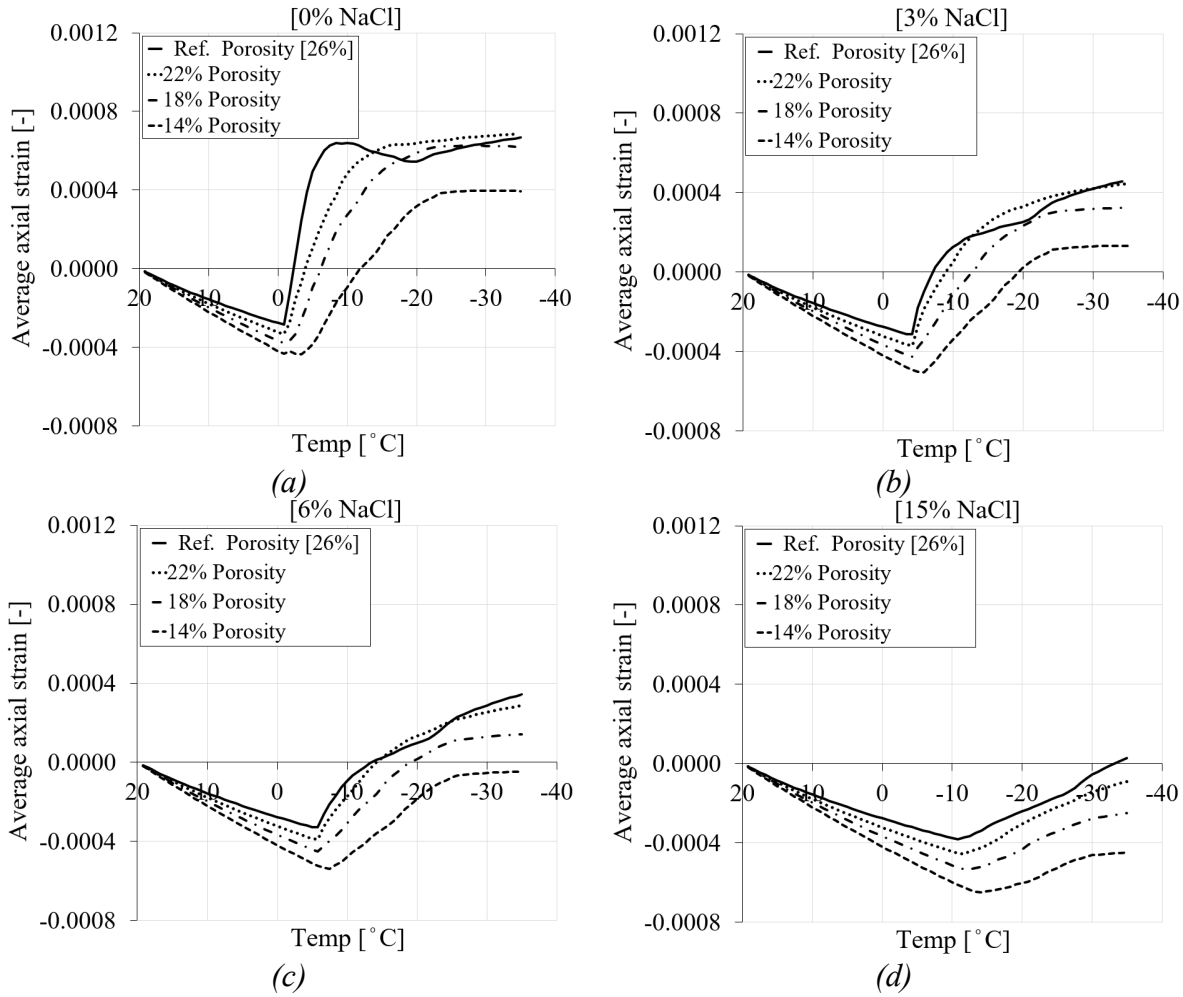


*Fig. 21: The comparison between the freezing strains of the reference porosity and liquid water permeability and three selected values based on Table 5 for PI cement paste during the first cooling phase (a) pure water (b) 3 % NaCl (c) 6 % NaCl (d) 15 % NaCl*

The evaluation of the numerical results for the first cooling phase for PI hardened cement paste showed that the modified porosity and the corresponding liquid water permeability influence the liquid and ice pressure generated during the freezing process. It should be noted that a modified porosity volume indicates a different pore structure and behavior of the material. While the relationship between porosity and liquid water permeability is not always straightforward, as other factors can also affect the permeability of the hardened cement paste, in general, lower porosity results in lower liquid water permeability because there are fewer pathways for water to flow through. This phenomenon leads to the build-up of higher fluid pressure compared to a more porous material. Fig. 22 shows the liquid pressure for four porosity cases according to Table 5 for pure water.

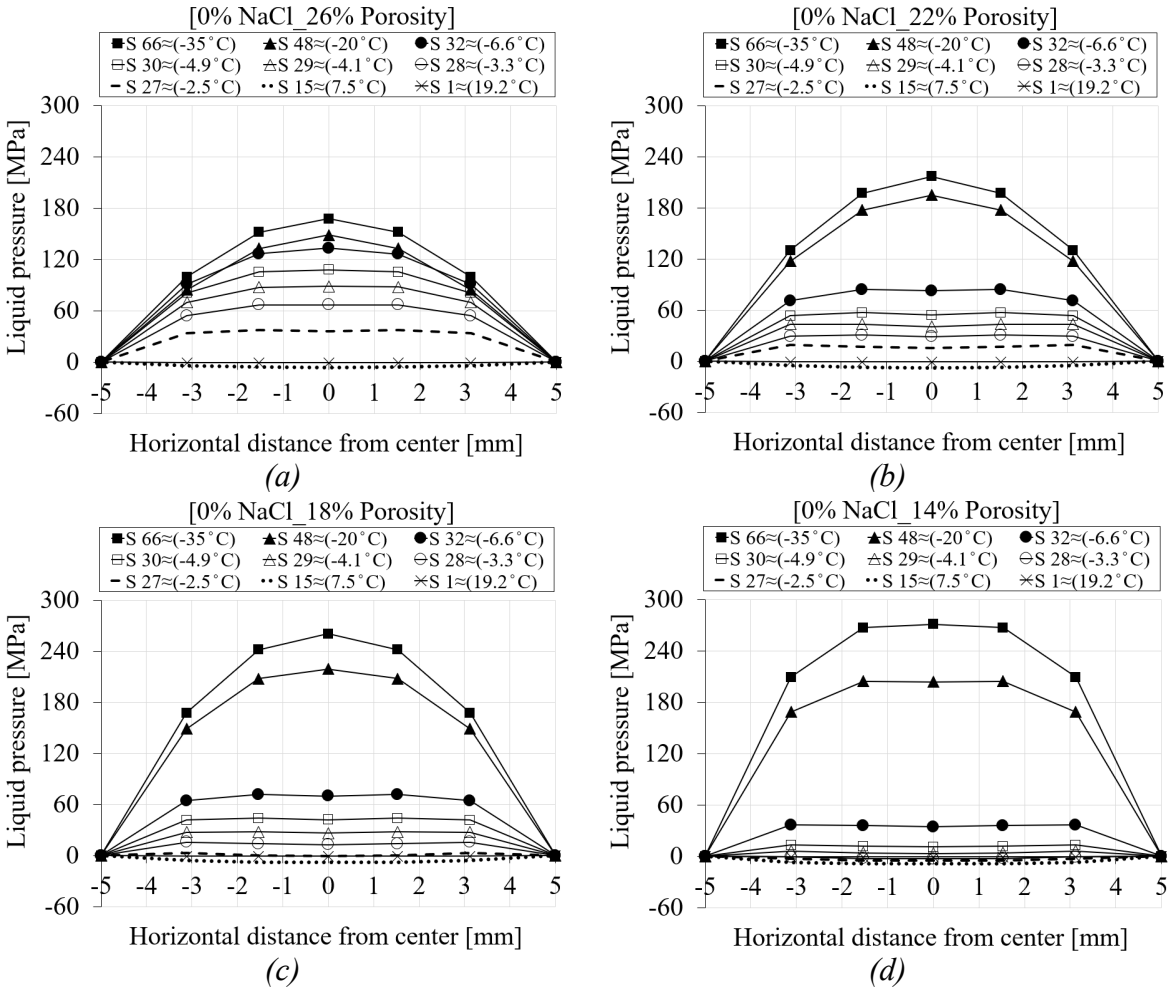


*Fig. 22: The comparison between the liquid pressure of the reference porosity and liquid water permeability and three selected values based on Table 5 for PI cement paste during the first cooling phase (a) 26 % porosity (b) 22 % porosity (c) 18 % porosity (d) 14 % porosity*

Fig. 23 shows the ice pressure for four porosity cases for pure water. The results in Figs. 23a to 23c show no significant difference in ice pressure, but the ice pressure in Fig. 23d is slightly higher for 14 % porosity than in the other cases. This is likely related to the higher proportion of smaller pores (Fig. 18) compared to the other porosity curves, resulting in less space available for ice expansion during the freezing process, leading to higher pressure.

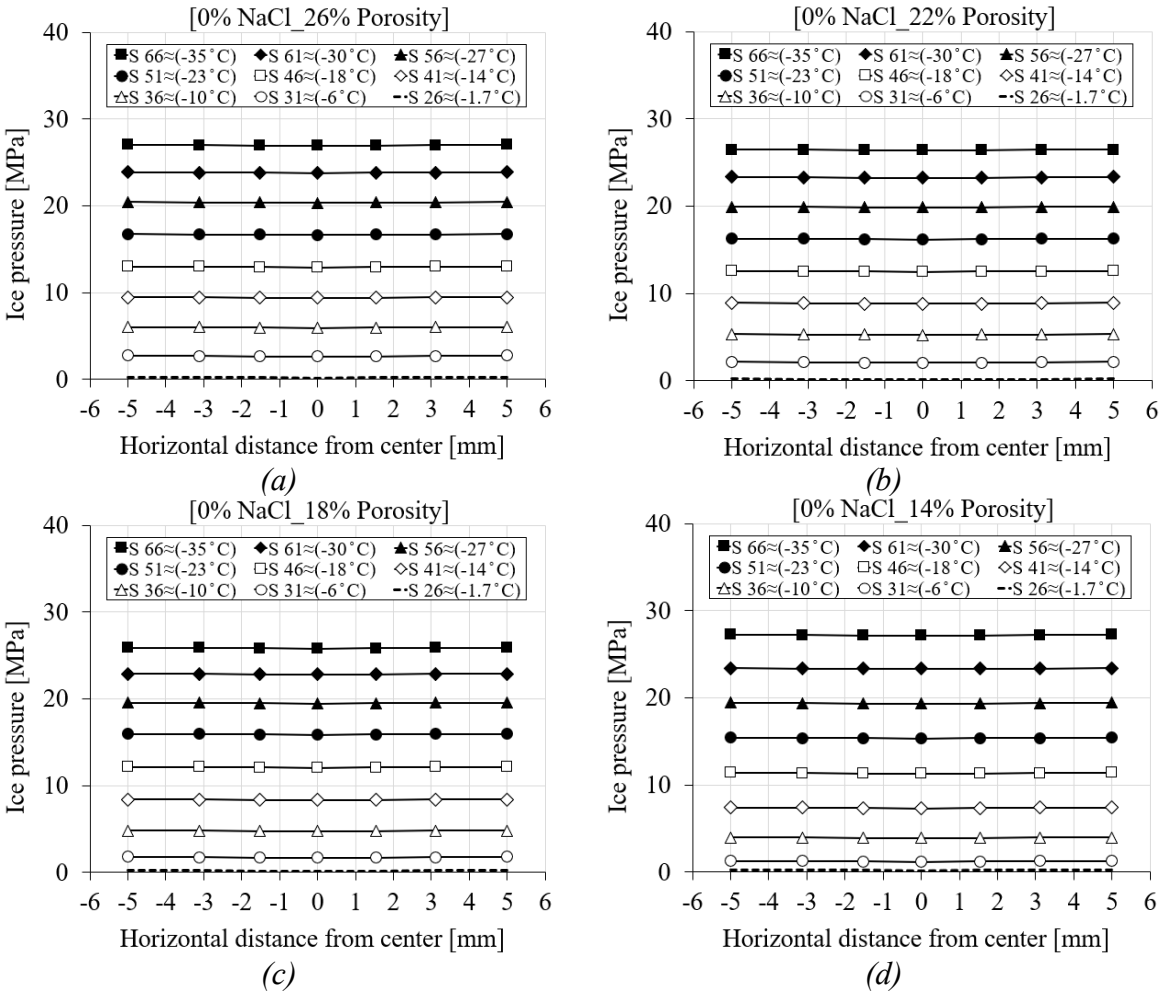


*Fig. 23: The comparison between the ice pressure of the reference porosity and liquid water permeability and three selected values based on Table 5 for PI cement paste during the first cooling phase (a) 26 % porosity (b) 22 % porosity (c) 18 % porosity (d) 14 % porosity*

Comparison of the results of cases 1 and 2 shows that for a fixed overall porosity and pore size distribution, changes in water permeability can significantly affect pore pressure and freezing strain. Lower permeability to liquid water reduces the rate at which water moves through the pores, resulting in higher pressure. However, if one reliably changes the permeability to liquid water and the pore size distribution based on the overall porosity of the material, the cement paste with lower permeability will experience more contraction and less expansion during the freezing process.

# 5. CONCLUSIONS

In the present study, the freezing behavior of two saturated cement pastes (PI, PII) with different chloride concentrations was numerically investigated. The analysis was performed using the coupled 3D hygro-thermo-mechanical FE model implemented in the in-house code MASA [22]. The mathematical formulation of the model is based on the theory available in the literature [14]. The mechanical part of the model is based on the microplane theory considering the linear elastic behavior of the material. The coupling between the mechanical and non-mechanical processes is ensured by using the "staggered" solution procedure. After the calibration and validation of the model, a parametric study was carried out to investigate the effect of the liquid water permeability, total porosity and pore size distribution on the pore pressure and deformation of the PI cement paste. The results can be summarized as follows:

(i) The FE model can realistically replicate the freezing behavior of the investigated cement pastes, in terms of generated pore pressure and consequent material deformation. A good agreement is observed between the here obtained results and those (numerical and experimental) reported in [8];

(ii) For cement paste with high porosity and water-cement ratio (PI), the deformation shows contraction followed by expansion. However, in the denser cement paste with lower porosity (PII), only contraction is observed due to the denser structure of the paste as well as smaller pore sizes, i.e. no freezing occurred;

(iii) Pore pressure is mainly generated in PI cement paste. The results showed that the maximum pore pressure is observed in the center of the specimen with gradual reduction towards the surface of the specimen.

(iv) The amount of chloride concentration in the pore solution has significant influence on the generated pore pressure and deformation. This is due to a delay in the freezing process;

(v) Based on the experimental results in [8], the freezing point of the pore solution for the same chloride concentration has been modified in the model, with consequent delay of freezing process and better agreement with the experimental deformation curves shown in [8];

(vi) The results of the parametric study of the liquid water permeability show that by decreasing the value of this parameter, for the same amount of chloride concentration, the pore pressure increases which results in higher deformation. Differently, an increase in permeability leads to lower pore pressure and deformation. However, the generated ice pressure is independent of water permeability, which is only dominant during the liquid phase of the pore solution;

(vii) The parametric study on the liquid water permeability, total porosity and pore size distribution showed that the total porosity and its corresponding liquid water permeability can influence the liquid pressure and freezing deformation. However, the results did not show a significant difference in ice pressure. As total porosity decreases, permeability to liquid water decreases, resulting in higher liquid pressure. However, cement pastes with lower porosity showed higher contraction and lower expansion during freezing, which can be attributed to the influence of thermal contraction during the cooling phase;

(viii) Finally, this study has focused on the freezing behavior of cement pastes during the first cooling phase. However, the main challenge in simulating frost action in cementitious materials is related to cyclic freeze-thaw loading which will be addressed in future investigations. Understanding the relationship between liquid permeability, porosity and changes of the pore structure during freeze-thaw attack is essential for accurately predicting the performance of the cement paste under cyclic freeze-thaw loading.

## REFERENCES

[1] BEAUDOIN, J.J.; MACINNIS, C.: *The mechanism of frost damage in hardened cement paste*. Cem Concr Res (1974) 4(2):139–47

[2] POWERS, T.C.: *The air requirement of frost-resistant concrete*. Proc Highway Res. Board (1949) 29:184–211

[3] SCHERER, G.W., VALENZA, J.J., YOUNG, F., SKALNY, J.: *Mechanisms of frost damage, materials science of concrete VII*. (2005) American Ceramic Society

[4] NG, K., SUN, Y., DAI, Q., YU, X.: *Investigation of internal frost damage in cementitious materials with micromechanics analysis, SEM imaging and ultrasonic wave scattering techniques*. Constr Build Mater (2014) 50:478–85

[5] WARDEH, G., MOHAMED, M., GHORBEL, E.: *Analysis of concrete internal deterioration due to frost action*. J Build Phys (2011) 35(1):54–83

[6] PIGEON, M., REGOURD, M.: Effects of freeze-thaw cycles on the microstructure of hydration products, Durability Build. Mater. 4 (1986) 1–19

[7] VERBECK, G., KLIEGER, P.: *Study of salt scaling of concrete*. Highw Res Board Bull (1957) 150:1-17

[8] ZENG, Q., FEN-CHONG, T., LI, K.: *Freezing behavior of cement pastes saturated with NaCl solution*, Construction and Building Materials 59 (2014) 99–110

[9] WANG, Y., YANG, W., GE, Y., LIU, P., ZHANG, A.: *Analysis of freeze-thaw damage and pore structure deterioration of mortar by low-field NMR*, Construction and Building Materials 319 (2022) 126097

[10] ZHANG, K., ZHOU, J., YIN, Z.: *Experimental Study on Mechanical Properties and Pore Structure Deterioration of Concrete under Freeze–Thaw Cycles*, Materials (2021), 14, 6568. https://doi.org/10.3390/ma14216568

[11] POWERS, T.C.: *A working hypothesis for further studies of frost resistance of concrete*, J. Am. Concr. Inst. 41 (1945) 245–272

[12] POWERS, T.C., HELMUTH, R.A.: *Theory of volume changes in hardened Portland cement paste during freezing*, Portland Cement Association, (1953) Skokie, Ill

[13] BAŽANT, Z.P., CHERN, J.C., ROSENBERG, A.M., GAIDIS, J.M.: *Mathematical model for freeze-thaw durability of concrete*, J. Am. Ceram. Soc. 71 (1988) 776–783

[14] ZUBER, B., MARCHAND, J.: *Modeling the deterioration of hydrated cement systemsexposed to frost action – Part 1: description of the mathematical model*, Cem. Concr. Res. 30 (2000) 1929–1939

[15] ZUBER, B., MARCHAND, J.: *Predicting the volume instability of hydrated cement systems upon freezing using poro-mechanics and local phase equilibria*, Mater. Struct. 37 (2004) 257–270

[16] YANG, R., LEMARCHAND, E., FEN-CHONG, T., AZOUNI, A.: *A micromechanics model for partial freezing in porous media*, Int. J. Solids Struct. 75–76 (2015) 109–121

[17] LIU, L., YE, G., SCHLANGEN, E., CHEN, H., QIAN, Z., SUN, W., BREUGEL, K.: *Modeling of the internal damage of saturated cement paste due to ice crystallization pressure during freezing*, Cem. Concr. Compos. 33 (2011) 562–571

[18] JIANG, W., SHEN, X., XIA, J., MAO, L., YANG, J., LIU, Q.: *A numerical study on chloride diffusion in freeze-thaw affected concrete*, Construction and Building Materials 179 (2018) 553–565

[19] RHARDANE, A., SLEIMAN, S., ALAM, S., GRONDIN, F.: *A quantitative assessment of the parameters involved in the freeze–thaw damage of cement-based materials through numerical modelling*, Construction and Building Materials 272 (2021) 121838

[20] OLSEN, M.P.J.: *Mathematical modeling of the freezing process of concrete and aggregates*. Cem. Concr. Res. (1984), 14, 113–122

[21] OŽBOLT, J., ORŠANIĆ, F., BALABANIĆ, G., MARIĆ, M.: *Modeling damage in concrete caused by corrosion of reinforcement: coupled 3D FE model*, Int. J. Fract. (2012) 178: 233-244

[22] OŽBOLT, J.: *MASA–"Macroscopic Space Analysis"*, Internal Report, Institute für Werkstoffe im Bauwesen, Universität Stuttgart, Germany (1998)

[23] OŽBOLT, J., LI, Y., KOŽAR, I.: *Microplane model for concrete with relaxed kinematic constraint*, International Journal of Solids and Structures 38 (2001) 2683-2711

[24] COUSSY, O.: *Poromechanics of freezing materials*, Journal of the Mechanics and Physics of Solids 53 (2005) 1689–1718

[25] DUAN, A., CHEN, J., JIN, W.: *Numerical Simulation of the Freezing Process of Concrete*, J. Mater. Civ. Eng. (2013) 25:1317-1325

[26] FAGERLUND, G.: *Determination of pore-size distribution from freezing-point depression*, Matériaux et Construction volume 6, (1973) pages 215–225

[27] ZENG, Q.: *Poromechanical behavior of cement-based materials subjected to freeze-thaw actions with salts: modeling and experiments*, thesis, HAL Id: tel-00688191, https://tel.archives-ouvertes.fr/tel-00688191, Submitted on 17 Apr 2012

[28] LIDE, D.R.: *CRC handbook of chemistry and physics*, 84th Ed., CRC Press, (2003) Boca Raton, FL

[29] LIN, C., LEE, L.: *A two-ionic-parameter approach for ion activity coefficients of aqueous electrolyte solutions*, Fluid Phase Equilibria 205 (2003) 69–88

[30] ZIENKIEWICZ, O.C., TAYLOR, R.L.: *The Finite Element Method - the Basis*, (2000) Vol. 1. fifth edition, Butterwirth-Heinemann

[31] BELYTSCHKO, T., LIU, W.K., MORAN, B.: *Non-linear finite elements for continua and structures*, John Wiley & Sons Ltd (2001)

[32] LI, K., XU, L., STROEVEN, P., SHI, C.: *Water permeability of unsaturated cementitious materials: A review*, Construction and Building Materials 302 (2021) 124168

[33] ZENG, Q., LI, K., FEN-CHONG, T., DANGLA, P.: *Effect of porosity on thermal expansion coefficient of cement pastes and mortars*, Construction and Building Materials 28 (2012) 468–475

[34] COUSSY, O., MONTEIRO, P.J.M.: *Poroelastic model for concrete exposed to freezing temperatures*, Cement and Concrete Research 38 (2008) 40–48